Title

Cantor-derived medium-entropy alloys: bridging the gap between traditional metallic and high-entropy alloys

Authors

Da Costa Garcia Filho, Fabio
Ritchie, Robert O
Meyers, Marc André
et al.

Publication Date

2022-03-01

DOI

10.1016/j.jmrt.2022.01.118

Peer reviewed

Available online at www.sciencedirect.com

jmr&t Journal of Materials Research and Technology

journal homepage: www.elsevier.com/locate/jmrt

Original Article

Cantor-derived medium-entropy alloys: bridging the gap between traditional metallic and high-entropy alloys

Fabio Da Costa Garcia Filho [a,b,*], *Robert O. Ritchie* [c], *Marc André Meyers* [b], *Sergio Neves Monteiro* [a]

[a] *Department of Materials Science, Military Institute of Engineering, Rio de Janeiro, RJ, 22290-270, Brazil*
[b] *Department of Mechanical and Aerospace Engineering, University of California, San Diego, CA, 92093, United States*
[c] *Materials Sciences Division, Lawrence Berkeley National Laboratory, and Department of Materials Science and Engineering, University of California, Berkeley, CA, 94720, United States*

ARTICLE INFO

Article history:
Received 24 October 2021
Accepted 20 January 2022
Available online 1 February 2022

Keywords:
High-entropy alloys
Medium-entropy alloys
Mechanical properties
Microstructure
Cantor alloy

ABSTRACT

The year 2004 marked the beginning of a new era in the design of metallic materials, as the concept of multiple principal component alloys, commonly known as High-Entropy Alloys (HEAs), was proposed by Cantor and Yeh. The unexpected single-phase microstructure, instead of the expected brittle intermetallic compounds, was attributed to the large entropy of mixing and immediately caught the attention of the scientific community. Today, HEAs are considered important advanced materials and a broad range of alloys using nominally the same design principle have been investigated. Despite that, the CrMnFeCoNi (Cantor) alloy stands out as the most successful HEA due to its outstanding mechanical properties and microstructure. In this scenario, variants of the Cantor alloy, named medium-entropy alloys (MEAs), are gaining significant interest as they display a better industrial potential than both HEAs and traditional alloys. These variants of the Cantor alloy with only three or four main elements result in 15 possible combinations. The microstructure of these alloys is discussed in terms of advanced characterization as well as thermodynamic parameters and computational simulation. Their phase stability is addressed over a wide range of temperatures and strain rates. The mechanical properties, especially the fracture toughness, of the CrFeCoNi and CrCoNi alloys have been reported to be even superior to those of the Cantor alloy and most modern engineering alloys. This is associated with the formation of a continuous sequence of strengthening mechanisms, including hierarchical twin networks, which serve to prolong the strain hardening. The present article reviews and critically assesses, for the first time, recent advances in these Cantor-derived MEAs.

* Corresponding author.
E-mail address: fabiogarciafilho@gmail.com (F.D.C. Garcia Filho).
https://doi.org/10.1016/j.jmrt.2022.01.118

1. Introduction

In 2004, the Materials Science field took a major step towards the unknown hyper-dimensional composition space through the development of a new strategy for designing metallic alloys. Historically, metallic alloys were made with one or two principal elements combined with several minor alloying elements that were added in concentrations as low as few atomic percent to enhance the properties of the material. This basic strategy persisted for a long time and led to the development of a broad range of well-known engineering materials such as: bronze, steels, aluminum alloys, stainless steels, titanium alloys, nickel alloys and many others. This strategy stimulated the development by the scientific community of the foundational knowledge of physical metallurgy, phase diagrams, mechanical behavior, and microstructure of metallic alloys, which are the basis of materials science engineering. In principle, the development of alloys using this approach is predicated on the avoidance of complex microstructures and the precipitation of intermetallic compounds, which can result in compromised mechanical behavior. The formation of extraneous phases, such as Laves, Sigma, Chi, is also an undesirable presence. Indeed, when the concentration of minor elements is generally increased, the occurrence of intermetallic compounds and phases is often observed. Thus, the microstructural and chemical complexity of the alloy is also increased, as for example seen in TWIP and TRIP steels or in titanium alloys with a higher content of Mo and W, in comparison to traditional alloys. In this regard, He et al. [1] showed that the development of metallic materials over the ages followed a trend of increasing chemical alloy complexity, an approach which in many cases has resulted in the enhancement of properties.

The traditional design approach, however, was about to change when two research groups, one from the University of Oxford in England and the other at the National Tsinghua University in Taiwan, independently proposed a new strategy based on the notion of multiple principal elements to design metallic alloys. Cantor revealed in a lecture in 2017 that he already had the paper on such alloys [2] sitting on his drawer for over a decade. It is also known that Yeh had already wondered about this possibility in the late 1990's, but it was a series of theses that resulted in his five publications in 2004 [3–7]. The 2004 Cantor et al. and Yeh et al. papers officially initiated a new era of this strategy for metallic alloys. Cantor et al.'s [2] objective was to "investigate the unexplored central region of multicomponent alloy phase space." They initially investigated alloys with 16 and 20 main elemental constituents, but both of these alloys were shown to be multiphase and brittle. However, a single face-centered cubic (*fcc*) primary phase containing many elements but especially rich in Co, Cr, Fe, Mn, and Ni caught their attention. Accordingly, they decided to further investigate the equiatomic five-element alloy CrMnFeCoNi; this single-phase *fcc* alloy was to become known as the *Cantor alloy*. The unexpected multicomponent single phase instead of several intermetallic phases, as one might anticipate, was exciting but was slow to gain much attention of the scientific community. What could be missing for this alloy strategy to become a hit in Materials Science

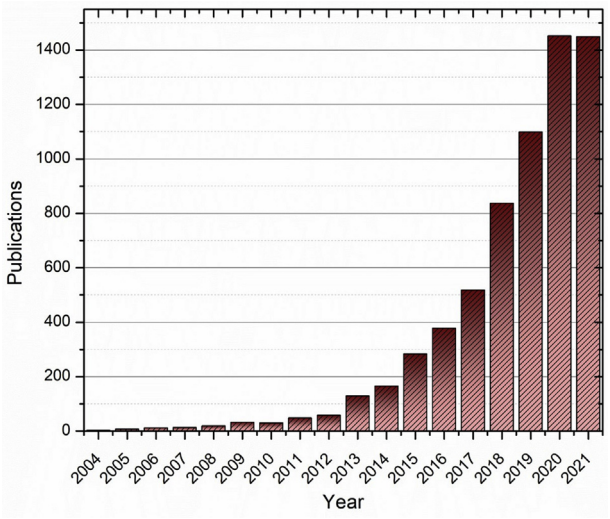

Fig. 1 – Evolution of the number of publications by year regarding the keywords "HEAs", "MPEAs", and "CCAs" according to Scopus database.

field? The answer came as a "catchy" name, which was proposed by Yeh et al. [3]. He suggested that alloys with greater number of principal elements would form random solid solutions easier than intermetallic compounds during solidification due to a higher configurational entropy. This statement was later discouraged by Otto et al. [8] who pointed out that the role of configurational entropy was non-predominant in predicting if the alloy will form a thermodynamically stable single-phase solid solution. Nevertheless, the "catchy" name stayed: High-Entropy Alloys (HEAs).

The relevant questions raised in the following years were: "What exactly are HEAs? How are they defined?". The two main ways to answer these questions are the composition- and entropy-based definitions. The composition-based definition was proposed in the first concept paper about HEAs by Yeh et al. [3]. The authors defined that HEAs should have at least five principal elements and that these principal elements would be considered those with atomic percentage between 5 and 35%. Such definition also dictated that no element should exceed 35 at.% and that three different types of HEA systems would be considered as possible: (i) one equimolar composition, (ii) several non-equimolar compositions, and (iii) compositions with minor additions of other elements. On the other hand, the entropy definition states that HEAs as having configurational entropy larger than 1.5*R* in the random-solution state, where *R* is the gas constant [9]. At the same time, those alloys exhibiting values between 1*R* and 1.5*R* should be addressed as medium-entropy alloys (MEAs) and those lower than 1*R* as low-entropy alloys (LEAs). Unfortunately, these definitions, which we expected to enlighten the HEA field, instead provoked more debate about the nature of HEAs that lingers until today. Yeh [10], in his book devoted to the physical metallurgy of HEAs, suggested that "even those alloys close to any of the two definitions could be regarded as HEAs." With that, one finds papers that investigate alloys still claimed to be HEAs but where the amount of one of the elements is higher than 35 at.% or where alloys have less than

five main elements. In addition, there are those researchers that prefer to use other terms such as "multiple principal elements alloys (MPEAs)" or "complex concentrated alloys (CCAs)", rather than HEAs. One might agree that this could lead to some misunderstanding about the subject. Miracle and Senkov [11] addressed this issue as an "unproductive controversy" since this discussion may draw away researchers' attention from the potential scientific and practical benefits hidden in the vastness of the hyper-dimensional composition space. In fact, they are right about this "vastness of the hyper-dimensional composition space" as a large number of works have been published since the discovery of HEAs. Searching the keywords "HEAs", "MPEAs", and "CCAs" in the main research database, it is possible to verify the evolution of the number of publications over the years as shown in Fig. 1.

This amazing number of publications includes studies that investigate physical metallurgy, development of new compositions as well as physical properties, mechanical behavior, and many other characteristics of HEAs. Several review papers were published over the years to keep up with the published investigations but also to present some clarification about the main concepts of the field [11–21].

The ripening knowledge about HEAs, achieved after 17 years since their first appearance, reveals that only a few HEAs actually exhibit single-phase microstructures. CrMnFeCoNi [2], HfNbTaTiZr [22], and DyGdHoTbY [23] are, respectively, classical *fcc*, body-centered cubic (*bcc*) and hexagonal close-packed (*hcp*) single-phase HEAs. Zhang et al. [16] discussed that, due to the rareness of single-phase HEAs, the research focus on single-phase and more than five principal element alloys has been changing in last few years. They suggest that expanding the research scope of HEAs toward non-equimolar complex phases will affect the classical definition of HEAs but will also facilitate material design and development. This change in approach is now referred as the second generation of HEAs, where the alloy must be based on at least four main elements and dual or complex phases are also accepted. Indeed, this change of perception does bolster the development of new alloys. Interstitial elements such as carbon, oxygen, nitrogen, and boron have been introduced into HEAs to enhance their mechanical properties [24–27]. For example, Wang et al. [28] showed that carbon triggers the microband-induced plasticity effect in a CrMnFeAlNi HEA by increasing the lattice friction stress. Lei et al. [29] reported that in addition to interstitial strengthening effects, oxygen forms complex structures in a TiZrHfNb alloy that promote double cross-slip and dislocation multiplication via formation of Frank–Read sources, associated with strain hardening during deformation. The precipitation of hard intermetallic phases, such as μ, σ and Laves also becomes a possibility for this new generation of HEAs [30–32]. Twinning-induced plasticity (TWIP) and transformation-induced plasticity (TRIP) effects have been reported in non-equiatomic HEAs [33–36].

Despite the mindset change in research direction in recent years with the second generation of HEAs, a rather "romantic" approach for investigating HEAs continues to linger in research papers, as the single-phase stability of the HEAs still raises a lot of attention. The Cantor alloy still retains a special place and continues to be one of the most investigated HEAs. In this scenario, other MEA variants of the Cantor alloy started attracting interest owing to the fact that many still displayed, and sometimes exceeded, some of the exceptional characteristics of HEAs. Additionally, these variants offer other advantages; they exhibit a better industrial potential due to ease of manufacture and lower costs than either HEAs or several traditional alloys, and academically they are far more amenable to modeling using first-principles atomistic simulations [37]. Indeed, the Cantor alloy appears to provide the foundation of a large number of alloys. However, when considering only medium-entropy equiatomic compositions derived from the Cantor composition, there are only 15 possibilities. The objective of this brief review is to critically assess recent research that discuss alloys that are derived from the Cantor HEA but with only three or four main elements. The importance of such alloys presented herein lies in their exceptional properties, microstructure, and potential applications.

2. Medium-entropy alloys derived from the CrMnFeCoNi system

2.1. *Phase formation*

Among the HEAs, the Cantor alloy is known as one of the few to crystallize as a single-phase *fcc* solid solution and one that displays a remarkable synergy in strength and ductility which is progressively enhanced at cryogenic temperatures. Several medium-entropy alloys (MEAs) have been produced based on the combination of elements of the Cantor alloy: cobalt, chromium, iron, manganese, and nickel. If only equiatomic MEAs are considered with three or four main elements, then as noted the possible combinations of elements are restricted to 15 new alloys. However, if non-equiatomic configurations are considered, then the number of different alloys becomes unlimited. Considering four principal elements, five different alloys can be identified, while for three main elements ten possible combinations can be obtained. Figure 2 illustrates the possible combinations for these equiatomic MEAs based on the Cantor alloy.

One might wonder what is the lattice structure of these alloys, since at room temperature the nickel is *fcc*, iron and chromium are *bcc*, cobalt is *hcp* and manganese crystallizes as α-Mn. Yeh et al. [3] proposed that four core effects were used to describe the microstructure and properties of the HEAs. The

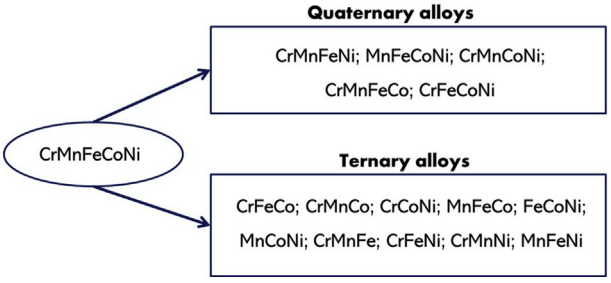

Fig. 2 – All the possible quaternary and ternary subsets of alloys that are derivatives of the quinary CrMnFeCoNi high-entropy (Cantor) alloy.

Table 1 – Empirical parameters for phase prediction in HEAs.

Empirical parameter	Formula	Criterion
Entropy of mixing	$\Delta S_{mix} = -R\sum c_i \ln c_i$	HEA if $\Delta S_{mix} \geq 1.5R$ MEA if $1 \leq \Delta S_{mix} < 1.5R$ LEA if $\Delta S_{mix} < 1.0R$
Enthalpy of mixing	$\Delta H_{mix} = \sum 4\omega_{ij} c_i c_j$	Solid solution phases formed if $-20 < \Delta H_{mix} < 5$ kJ/mol
Ω parameter	$\Omega = \frac{T_m \Delta S_{mix}}{\lvert \Delta H_{mix} \rvert}$	Solid solution phases formed if $\Omega \geq 1.1$
Atomic-size mismatch	$\delta = 100\% \sqrt{\sum c_i (1 - r/\bar{r})^2}$	Solid solution phases formed if $\delta \leq 6.6\%$
VEC	$VEC = \sum c_i VEC_i$	If VEC<6.87 bcc phases are stable, If VEC≥8 *fcc* phases are stable
Pauling electronegativity difference	$\Delta\chi_{Pauling} = \sqrt{\sum c_i (\chi_i^{Pauling} - \bar{\chi})^2}$	If $\Delta\chi^{Pauling} > 0.133$, *tcp* phases can be observed
Allen electronegativity difference	$\Delta\chi_{Allen} = \sqrt{\sum_{i=1}^{n} c_i (1 - \chi_i^{Allen}/\chi_a)^2}$	Only solid solution phases observed if $0.3 < \Delta\chi^{Allen} < 0.6$

(i) high entropy effect for thermodynamics; (ii) sluggish diffusion effect for kinetics; (iii) severe lattice distortion effect for structure; and (iv) a "cocktail" effect for properties. These are core effects that contribute principally to the characterization of HEAs. In fact, these effects are also present in the MEAs but were expected to influence to a lower degree [38]. Therefore, it is not hard to imagine that some of these MEAs may not crystalize as a single *fcc* phase, as the Cantor alloy, but as a multiphase material. Otto et al. [8], as earlier mentioned, discounted the predominant role of mixing entropy in the stabilization of single phase HEAs. Experimentally, they found that when replacing each constituent element of the Cantor alloy by another element, with a comparable room-temperature crystalline structure, size, and electronegativity but still keeping the same mixing entropy, multiple-phase structures were observed. Thus, this result provides evidence that the mixing entropy may not be the dominating factor for single-phase formation in multicomponent alloys. One then may ask what are the dominant parameters for predicting the phase formation in these alloys? Several researchers have addressed this issue by proposing different empirical parameters for predicting such single-phase solid-solution formation [39–48]. Some of these parameters are generalizations of the classical Hume-Rothery rules that deal with the formation of binary alloys based on atomic-size difference, electronegativity, and valence [49]. The atomic size mismatch (δ) and the mixing enthalpy (ΔH_{mix}) were considered to play an important role in the phase formation [50]. Subsequently, the ΔH_{mix} parameter was replaced by a thermodynamics-originated parameter [51,52]: this Ω parameter represents a competition between the enthalpy and entropy for single-phase stabilization. With the expectation of providing a more accurate prediction of whether the alloy, for example, would be *fcc* or *bcc*, Guo et al. [53] investigated the relevance of atomic bonding by the valence electron concentration parameter (VEC). They found that *fcc* phases are stable at higher VEC values while *bcc* phases are more likely to stabilize with lower VEC.

Zhu et al. [54] investigated the prediction parameters for phase formation in several alloys with respect to the addition of a specific element to that alloy. It was verified that the $(CrFeCo)_{(100-x)}Ni_x$ system was outside the solid-solution region proposed by Zhang et al. [50] in the $\Delta H_{mix} - \delta$ plot. Yet, when $x = 20$ the alloy is the equiatomic CrFeCoNi and forms a single phase. They suggested that near-zero values of ΔH_{mix} could not be a necessary condition for the single-phase formation, as the transition in the $(CrFeCo)_{(100-x)}Ni_x$ alloy system from a multi-phase CrFeCo alloy to a single-phase CrFeCoNi occurs despite the fact that ΔH_{mix} becomes more negative from its near-zero value. They also showed that for both alloy systems $(CrFeCo)_{(100-x)}Ni_x$ and $(MnFeCo)_{(100-x)}Ni_x$, the increase in Ni content leads to the stabilization of the *fcc* structure. Pertinent to this issue, Lyu et al. [55] addressed the effect of each element in multicomponent alloys. They pointed out that Ni has the ability to increase the production of the soft *fcc* phase, which could also be noticed through the reduction in hardness and increase in ductility.

Cui et al. [56] used several empirical criteria to determine the phase stability of the $MnFeCoNiTi_x$ system, with x ranging from 0 up to 1. In particular, the Cantor-derived MEA MnFeCoNi alloy was considered where $x = 0$. It was observed that for all investigated conditions, the calculated values meet the criteria for solid solution formation with ΔH_{mix} in the range from −20 to 5 kJ/mol [50] and the atomic size mismatch $\delta < 6.6\%$, as well as $\Omega \geq 1.1$ [51]. This is in accordance with the MnFeCoNi alloy, which is *fcc* and single phase; however, the same cannot be said for the $MnFeCoNiTi_{0.5}$ and $MnFeCoNiTi_{0.75}$ which were found to exhibit Laves phases in addition to the *fcc* matrix phase. As these alloys should be *fcc* and the VEC criterion [53] predicted otherwise, it is apparent that the proposed criterion is questionable from the perspective of predicting phase formation in these alloys. Laves phases are one of the topologically closed packed (*tcp*) phases and some elements, such as Co, Cu, Fe, Mo, Ni, Ti, V, Nb and Si, can exhibit a marked tendency for forming such *tcp* phases. To specifically address this latter issue in HEAs, Dong et al. [57] proposed an alternative criterion by suggesting that if the Pauling electronegativity difference ($\Delta\chi_{Pauling}$) were higher than 0.133, the *tcp* phases would be stable. Based on a study of this criterion for some 70 HEAs, they observed that

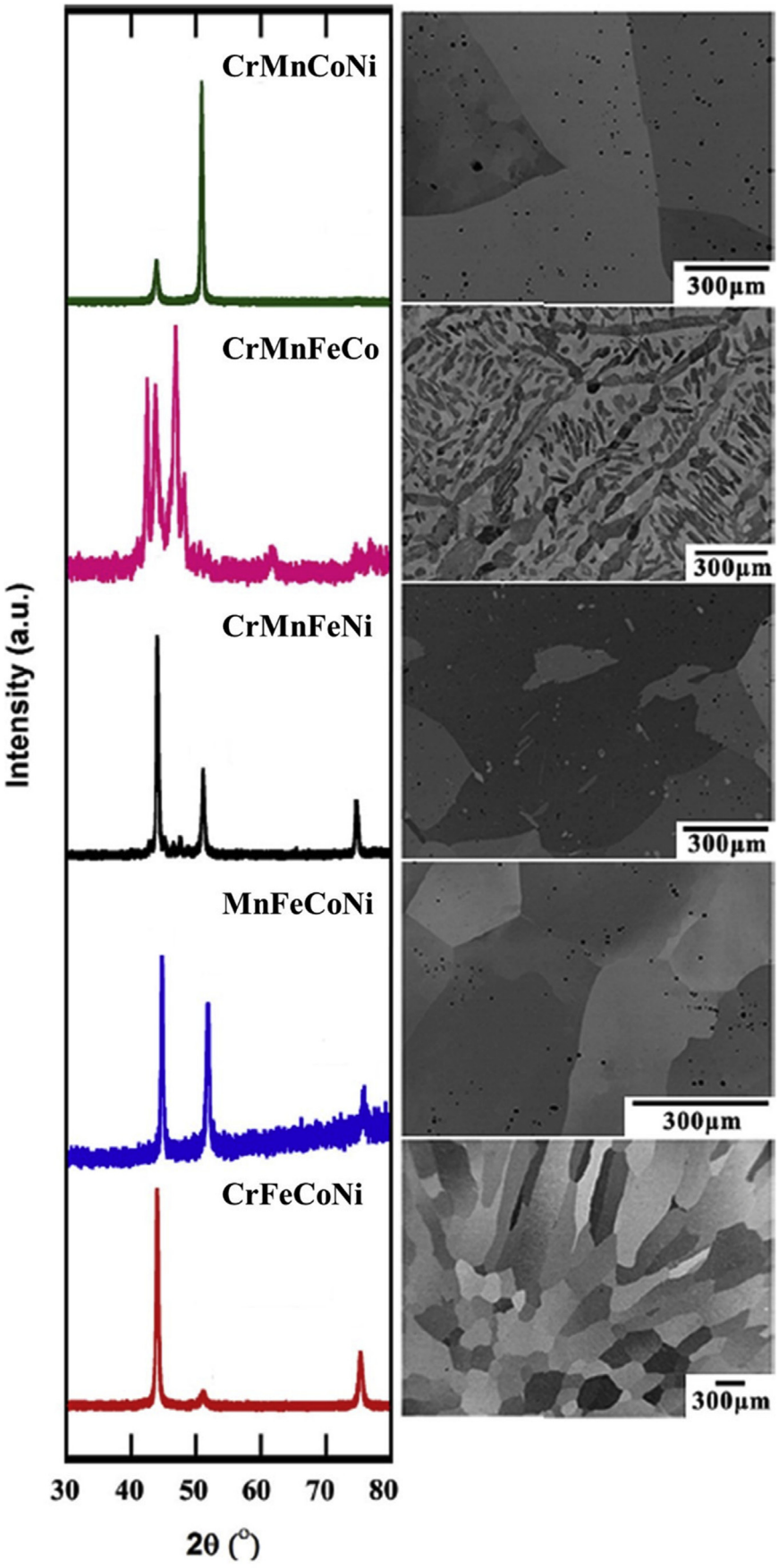

Fig. 3 – X-ray diffraction (XRD) patterns and back-scattered electron (BSE) images of the five quaternary equiatomic Cantor-derived MEAs, in the as-cast and homogenized condition. Adapted from [71].

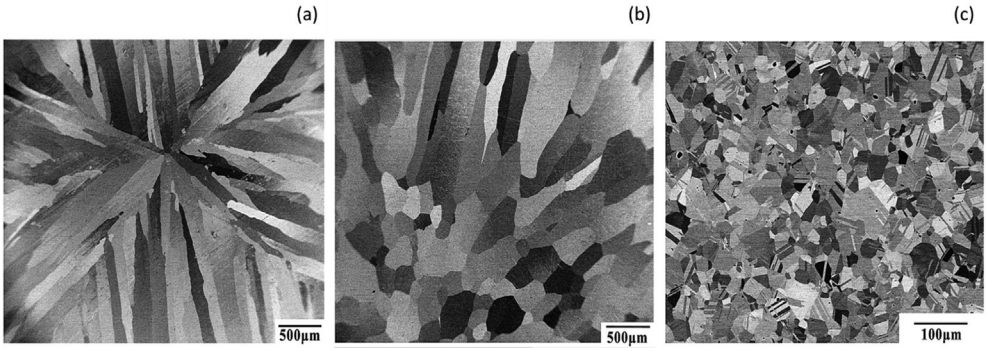

Fig. 4 – CrFeCoNi alloy microstructures (a) as-cast, (b) homogenized at 1200 °C for 24 h and (c) recrystallized by cold rolling and annealing at 900 °C for 1 h. Adapted from [71].

only alloys with appreciable amounts of elements that easily form *tcp* phases would conform to their criterion; Al-containing HEAs, for example, did not conform. However, the Dong et al. [57] criterion is also not valid. As an example, the calculated $\Delta\chi_{Pauling}$ for the MnFeCoNi alloys is 0.1429, which would imply that it should form some *tcp* phases, but this is in disagreement with experimental observations that show that it forms a single phase *fcc* alloy [58].

One concludes that the parameters affecting the prediction of phase formation in MEAs and HEAs are still somewhat uncertain. It is becoming clear that no single parameter, or combination of parameters, can precisely predict the phase formation for all possible multicomponent alloys. The lack of generalization might be associated with the understanding of the core effects, especially the competition between the thermodynamic parameters. The principal accepted and widely used empirical parameters for phase formation in multiple element alloys are summarized below in Table 1.

Another relevant aspect about phase formation, decomposition, phase transition and thermal stability of these MPEAs is the phenomenon of so-called "sluggish diffusion". In a recent review, Divinski et al. [59] analyzed results on both tracer and interdiffusion measurements and concluded that the idea of sluggish diffusion might be seen as ambiguous as the diffusion behavior would be strongly dependent on the element, matrix, and element concentration. The rather limited experimental information on diffusion transport in such alloys, especially for diffusion along grain and/or phase boundaries and/or for those alloys that do not crystallize as a single-phase *fcc* lattice, would also be relevant. Determination of diffusion coefficients in HEAs may be considered as a complex task due to a large number of components and limited number of systems which are stable enough to enable the long-term annealing necessary to conduct diffusion experiments. So far, three methods have been used to assess diffusivity in HEAs: radiotracer experiments [60–63], a quasi-binary approach [64–67], and optimization methods [68].

Vaidya et al. [69] were the first to measure diffusion along grain boundaries of Ni in chemically homogeneous CrFeCoNi MEA and CrMnFeCoNi HEA by radiotracer analysis using the ^{63}Ni isotope. CrMnFeCoNi exhibited a lower grain boundary diffusivity than the CrFeCoNi MEAs, but only below 1073 °C; this trend, however, was reversed with increase in temperature. The effects on the enthalpy and to the melting point by the addition of Mn corroborates with the hypothesis that increasing the number of elements alone does not lower the diffusion rates of the alloy. Instead, the nature of the element constituents plays a prime role. Similar investigations using radiotracer techniques were performed by Gaertner et al. [70] for both the CrFeCoNi and CrMnFeCoNi alloys to determine the tracer diffusion of all constituent elements at 1100 °C. The components exhibited significantly different diffusion rates, with Mn being the fastest element and Ni and Co being the slowest. Kucza et al. [68] used a combinatorial approach to determine the tracer diffusivities in a MnFeCoNi MEA. From the experimental results on the CrMnFeCoNi Cantor alloy at 1077 °C, they were able to predict the diffusion profile in the quaternary alloy, which indicated that the differences in diffusion kinetics between a five and four component system were practically negligible.

2.2. *Microstructure*

With an objective to better understand the possible formation of MEAs from the quinary CrMnFeCoNi HEA, Wu et al. [71] published an innovative report on the crystallization microstructure of quaternary, ternary and even binary alloys based on their constituents. Figure 3 presents scanning electron microscopy (SEM) images of the quaternary alloys as well as the corresponding X-ray diffraction (XRD) spectra. These alloys were prepared by arc melting using high-purity elements (>99.9% pure) and further homogenized in the range from 1100 to 1200 °C. Three compositions were found to be *fcc* (CrFeCoNi, MnFeCoNi, and CrMnCoNi), whereas the other two were described as being multiphase (CrMnFeNi and CrMnFeCo), as shown in Fig. 3.

The CrFeCoNi alloy has a single-phase *fcc* structure with a typical coarse as-cast microstructure, which could be associated with the arc melting process and homogenization (Fig. 3). This is one of the main reported Cantor-derived quaternaries MEAs due to its excellent combination of strength and ductility, as will be further discussed. The microstructure of this alloy can be modified by different processing procedures. Wu et al. [71], investigated the microstructural evolution during casting, homogenization, cold rolling, and annealing of the CrFeCoNi alloy. It was shown that the as-cast microstructure consists of

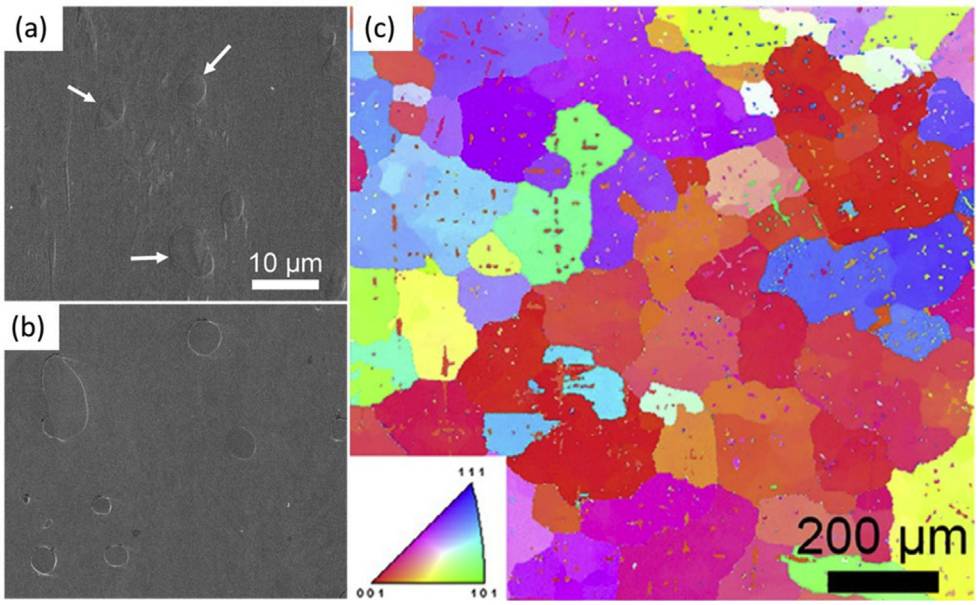

Fig. 5 – SEM micrographs of the CrMnFeNi alloy indicating the Cr-rich phase in the matrix (a) and (b); EBSD pole figure map displaying that the base material contains face-centered cubic (*fcc*) grains with Cr-rich body-centered cubic (*bcc*) grains throughout the specimen (c). Adapted from [75].

large elongated grains extending from the edges to the center, which were the result of the heat flow direction during solidification (Fig. 4 (a)). After homogenization at 1200 °C for 24 h, the elongated grains near the center of the casting were replaced by more equiaxed grains (Fig. 4 (b)). The alloy was subsequently rolled at room temperature in steps from 12.7 to 1.0 mm, without cross-rolling or intermediate annealing, which led to a major reduction in grain size. Further annealing at 900 °C produced a fully recrystallized microstructure composed of equiaxed grains with a high concentration of annealing twins (Fig. 4 (c)).

Other *fcc* quaternary MnFeCoNi and CrMnCoNi MEAs were also investigated by Wu et al. [72] and Ondicho et al. [73]. These CrMnCoNi and MnFeCoNi alloys were shown to exhibit recrystallized microstructures with equiaxed grains with mean size of 36 and 48 μm, respectively, similar to that observed for the CrFeCoNi alloy. Additionally, they reported on the influence of adding up to 60 at.% Fe to the CrMnCoNi, where they found that a single-phase *fcc* structure could be obtained after annealing at 900 °C for 2 h for the higher Fe content.

As for the non-single phase quaternary alloys CrMnFeCo and CrMnFeNi, no further information was given by Wu et al. [71] (Fig. 3). Kiran Kumar et al. [74] claimed that the equiatomic CrMnFeNi was not single-phase; to obtain a single-phase *fcc* alloy, they suggested that a non-equiatomic composition such as $Cr_{18}Mn_{27}$ $Fe_{27}Ni_{28}$ should be investigated, as the higher amount of Cr would promote the appearance of *bcc* Cr-rich or σ-phases [55]. Indeed, it was shown that this non-equiatomic alloy was single-phase *fcc*, although there was still a lack of confirmation about the equiatomic CrMnFeNi composition. Gigax et al. [75] recently investigated an equiatomic CrMnFeNi alloy, which was prepared by casting and then consolidation via hot isostatic pressing (the HIP parameters were 100 MPa pressure at 1200 °C for 4 h). The microstructure of this alloy was found to consist of *fcc* and *bcc* Cr-rich grains, with average sizes of, respectively, 232 and 9 μm (Fig. 5).

The other non-single phase quaternary alloy, CrMnFeCo, was experimentally investigated by Bracq et al. [76]. The alloy was processed by high-frequency electromagnetic induction melting, prior to annealing at 1000 °C and 1100 °C for up to 6 days under an inert atmosphere. XRD patterns showed that the CrMnFeCo alloy is composed of *fcc* and σ phases. In Fig. 6, the two phases can be observed by SEM and electron backscatter diffraction (EBSD) maps. The average size of the *fcc* grains was ~10 μm; they exhibited twins and the σ phase. The latter phase was shown to be Cr-rich (~33 at.%), while the *fcc* phase exhibited a slightly Cr-depleted composition. At 1000 °C, the volume percentage of the σ phase was 55%; by raising the annealing temperature to 1100 °C, the *fcc* phase became the majority phase at ~65%.

Laplanche et al. [77] investigated five ternary Cantor-derived MEAs, namely CrCoNi, CrFeNi, FeCoNi, MnCoNi, and MnFeNi, which were all produced by vacuum induction melting using pure elements (purity ≥99.9 wt.%). The cast ingots were homogenized for 48 h at 1200 °C for the alloys with no Mn- content and at 1100 °C for the alloys with Mn in their composition. Subsequently, the homogenized ingots were processed by rotary swaging until the reduction in the ingot diameter was equivalent to a true strain of 1.8. Finally, the alloys were recrystallized by annealing for 1 h at 900 °C followed by air cooling. Except for the ternary CrFeNi alloy, X-ray diffraction patterns of the recrystallized MEAs showed that the alloys were single-phase *fcc* structures with lattice parameters ranging from 0.357 nm in CrCoNi to 0.362 nm in MnFeNi. The fact that the single-phase alloys exhibited chemical homogeneity after the recrystallization may indicate that their microstructure is representative of the high-

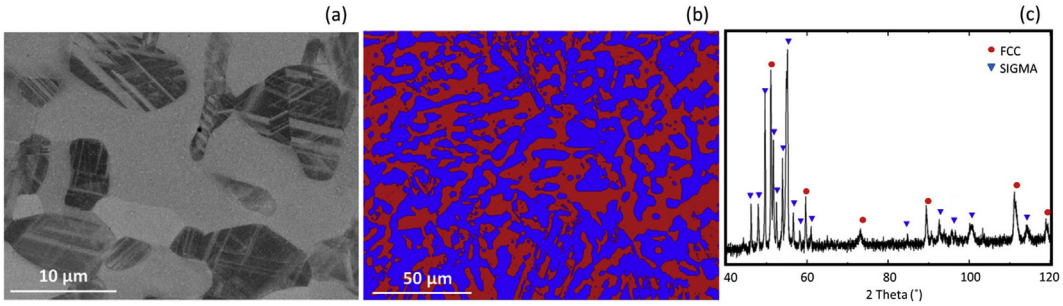

Fig. 6 – CrMnFeCo alloy (a) Back-scattered electron SEM image of twinned *fcc* grain embedded in the σ phase, (b) EBSD mappings illustrating the volume fraction distribution of *fcc* phase (red) and σ phase (blue), and (c) X-ray diffraction pattern. Adapted from [76].

temperature stable state. On the other hand, the CrFeNi alloy was found to exhibit a dual-phase microstructure comprising ~95% *fcc* and ~5% *bcc* phases (Fig. 7).

Dark particles at the grain boundaries are noticeable in the backscatter electron micrograph of the ternary CrFeNi alloy (Fig. 7 (a)). The phase map in Fig. 7(b) reveals that these particles have a *bcc* structure and form at the grain boundaries of the *fcc* phase. This suggested that the precipitation of the *bcc* phase particles could restrain grain-boundary movement during recrystallization, which is consistent with the smaller grain size of this alloy compared to the other single-phase *fcc* alloys investigated by Laplanche et al.. The fact that the CrFeNi alloy exhibits a dual-phase structure was also reported in ref. [71], although following homogenization these authors observed it to be single-phase *fcc*. This study concluded that the CrFeNi alloy was single-phase *fcc* for homogenization temperatures above 927 °C, but below this temperature it displayed a dual-phase (*fcc* + *bcc*) structure.

The other possible equiatomic ternary MEAs, namely CrFeCo, CrMnCo, MnFeCo, CrMnFe, and CrMnNi, were preliminarily assessed by Wu et al. [71]. All these alloys were found to be multi-phase in the as-homogenized condition for temperatures in the range from 1050 up to 1200 °C. These findings were shown to be in accordance with the phase stability information obtained from phase diagram calculations for ternary alloys. Nevertheless, the use of simulation for understanding the microstructure and phase stability of multicomponent alloys with more than three main elements is still an endeavor in progress that demands some degree of prudence; this is discussed below in Section 2.2.3.

2.2.1. *Long- and short-range order*

Recently, the randomness of the distribution of elements and its influence in these concentrated solid-solution alloys have been questioned. Lucas et al. [78] discussed the absence of a long-range chemical order (LRO) in the CrFeCoNi MEA. This phenomenon was investigated by anomalous X-ray diffraction (XRD) and neutron scattering measurements on samples in different conditions (quenched and aged) after homogenization at 1000 °C for 1 h. They compared the results of the MEAs with a binary $FeNi_3$, treated under the same conditions. The XRD spectra of the investigated materials are presented in Fig. 8. The annealed $FeNi_3$ alloy exhibited an ordered structure that can be identified by superlattice reflections. This characteristic was not observed for the quenched $FeNi_3$, which is known to exhibit a disordered structure. Similarly, the CrFeCoNi XRD spectra presented a pattern of disordered $FeNi_3$ for both heat treatment conditions. Nevertheless, Lucas et al. [78]

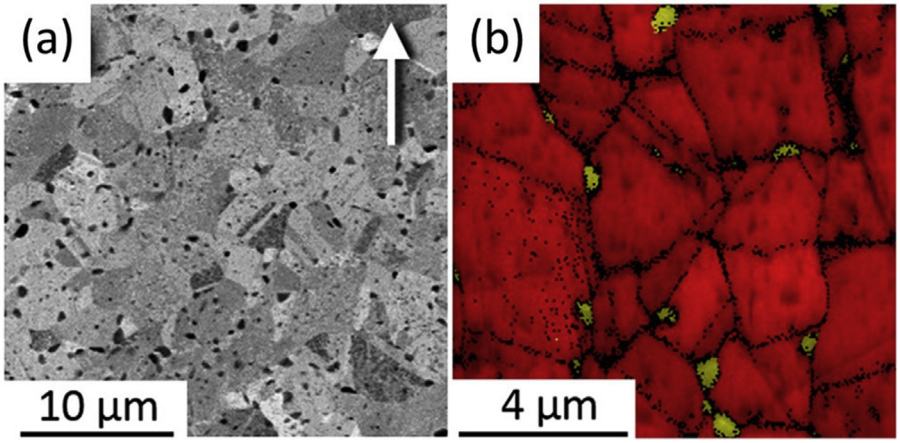

Fig. 7 – Microstructure of the CrFeNi dual-phase alloy. (a) Back-scattered electron SEM micrograph where the white arrow indicates the longitudinal axis of the recrystallized rod and (b) EBSD phase map where the red and yellow colors indicate *fcc* and *bcc* phases, respectively. Adapted from [77].

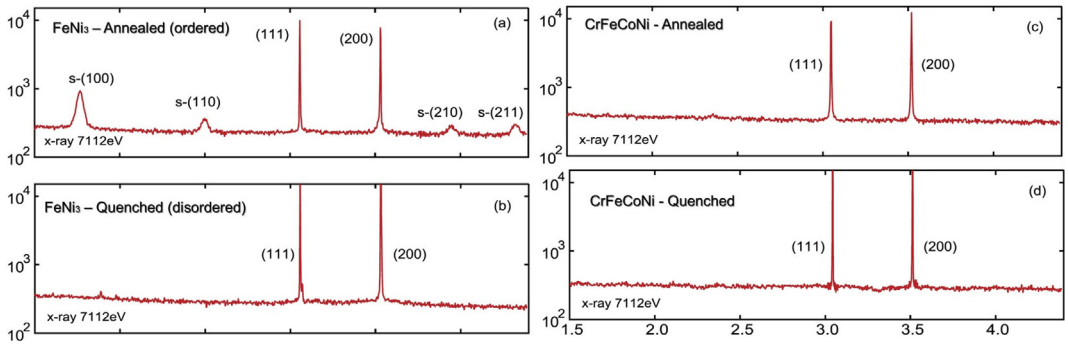

Fig. 8 – Anomalous x-ray diffraction for (a) annealed $FeNi_3$, (b) quenched $FeNi_3$, (c) annealed CrFeCoNi, and (d) quenched CrFeCoNi. Superlattice reflections indicative of local chemical ordering are denoted with an "s". Adapted from [78].

suggested that despite the lack of LRO, short-range chemical order (SRO) may be present. SRO can be understood as the correlation at small distances between chemical occupations of the atomic positions in the average crystal structure of the alloy, forming preferential inter-atomic neighborhoods. From a thermodynamic point of view, the driving force for this arrangement in multi-components alloys may have several causes: (i) fluctuation in the local strain; (ii) bonding state; or (iii) even electronic and magnetic interactions [79]. For solid-solution alloys, the effect of SRO on strengthening has been historically envisioned through the formation of either atomic pairs, triplets, or clusters, due to solute/solute interactions. These clusters can be considered as new, independent, and randomly distributed species that can interact with the dislocations, and thus play an important role in the mechanical and physical properties of alloys [80]. In fact, Ding et al. [81] performed a Density Functional Theory Monte Carlo-based study that demonstrated that chemical short-range order is thermodynamically favored in CrCoNi alloy and has a marked effect on the stacking fault energy. They further suggested that it could be tuned to affect the mechanical behavior of this alloy.

Ma et al. [82] recognized that characterizing SRO may be extremely difficult due to the chemical complexity induced by the multi-principal element approach in medium- or high-entropy alloys. Nevertheless, Zhang et al. [83] reported experimental observations, using energy-filtered transmission electron microscopy, of structural features that were associated with SRO in the CrCoNi MEA. CrCoNi specimens homogenized at 1200 °C and then aged at 1000 °C for 120 h followed by slow furnace cooling. They concluded that high-temperature aging leads to the formation of appreciable SRO in the CrCoNi MEAs. An increase of approximately 25% in the yield strength and an increment on the nanoindentation hardness were reported, which were attributed to SRO. Zhang et al. [83] suggested that despite lattice distortion and stacking fault energy (SFE) being widely proposed to explain the exceptional mechanical properties of the CrCoNi MEA [3,20], the SRO may be associated with changes in the static atomic displacements. Thus, it could represent a strong effect on dislocation plasticity which can be understood as atomic level tailoring of the alloy. Therefore, SRO is a critical feature for MEAs and tuning its degree might be considered an effective way for optimizing the mechanical properties of these alloys, as will be discussed in Section 2.3.2.

2.2.2. *Microstructural evolution*

The knowledge of phase stability in multi-component alloys is technologically relevant for applications over a wide range of temperatures where the decomposition into multiple phases can lead to modification of the mechanical properties [84]. The CrMnFeCoNi HEA has been shown to maintain its single-phase *fcc* crystalline structure over a large temperature range from cryogenic values up to the melting point without

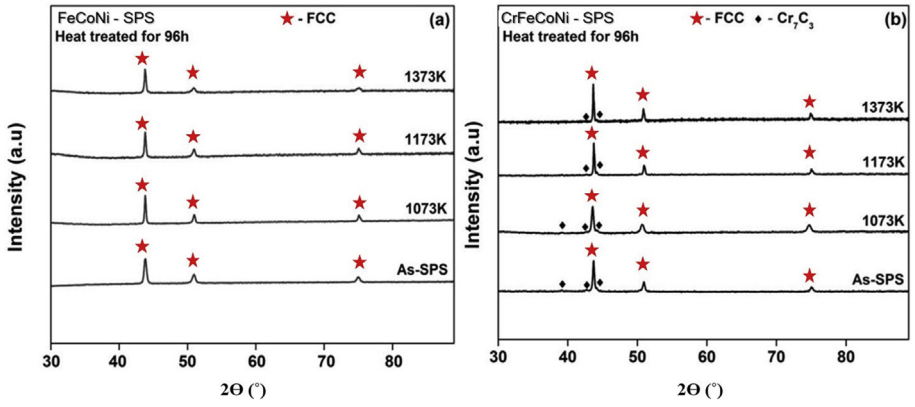

Fig. 9 – XRD patterns for SPS (a) FeCoNi and (b) CrFeCoNi alloy under different thermal exposure for 96 h. Adapted from [87].

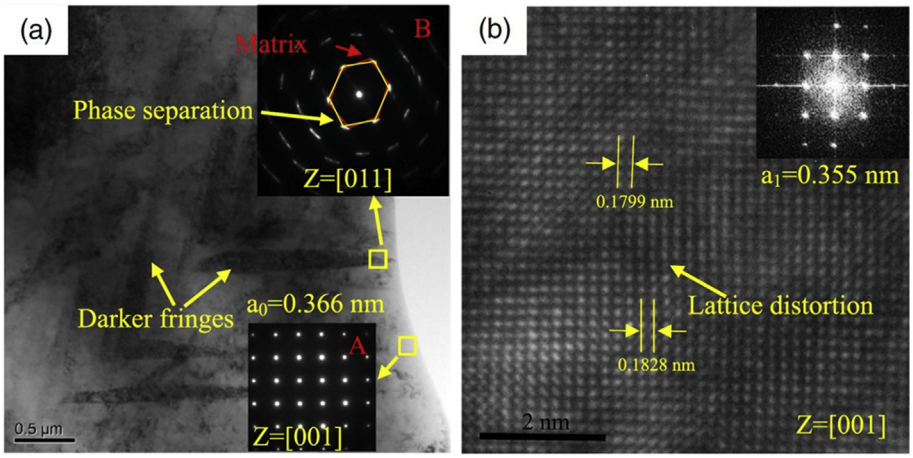

Fig. 10 – (a) Bright field TEM and (b) HRTEM images of the darker fringe in (a) of the CrFeCoNi alloy. The insets of (a) are selected diffraction patterns of the darker fringes area, marked A, and the matrix, marked B. Adapted from [92].

phase transformation [85]. Thus, one may expect that Cantor-derived MEAs might also display this remarkable phase stability throughout a wide range of temperatures. However, this should be regarded with caution, since Otto et al. [86] observed decomposition in the Cantor alloy after long thermal exposure times.

Vaidya et al. [87] investigated the phase stability of the FeCoNi and CrFeCoNi alloys. Figure 9 presents the XRD patterns of these two alloys heat treated for 96 h at different temperatures. This study concluded that the ternary FeCoNi alloy exhibited a single *fcc* phase with uniform distribution of elements and equiatomic composition, even after 96 h of heat treatment throughout the temperature interval of 800°–1100 °C (Fig. 9 (a)). The high stability of the alloy was related to the similar atomic sizes of the Co, Fe, and Ni as well as the enhanced solid solution exhibited by their binary alloys Co-Fe, Co-Ni, and Fe-Ni. For the quaternary CrFeCoNi, however, they observed an evolution of a Cr_7C_3 phase during heat treatment. This phase was associated with the tendency of Cr to form carbides during consolidation, which was possible due to a source of carbon in the processing of the alloys [88]. The carbon pick-up in mechanically alloyed powders was claimed to provide the thermodynamic driving force for the Cr_7C_3 formation, as predicted by the Ellingham diagrams, with reduced diffusion distances kinetically favoring the carbide evolution by the Cr-depletion of the *fcc* phase. It was shown that the Cr-carbide and Cr-oxide remained thermodynamically stable during the heat treatment and that no phase transformation of the *fcc* structure took place (Fig. 9 (b)). Furthermore, Praveen et al. [88] also reported that the fine distribution of Cr-rich carbides and Cr-rich oxides might prevent grain growth even at high homologous temperatures of ~0.68 of the melting temperature in this alloy. These are interesting results, as many studies have chosen CrFeCoNi as the base material for designing new alloys through the further addition of alloying elements, with the expectation of many potential applications [89,90]. It can therefore be concluded that minor additions of alloying elements to CrFeCoNi do not affect the phase stability of the base alloy.

Dahlborg et al. [91] investigated diffraction patterns of the CrFeCoNi alloy using high-energy X-rays. Contrary to what was expected, the as-cast alloy was found not to be single phase, instead consisting of two *fcc* phases with a difference in the lattice constant of 0.001 Å. Although they found that this surprising dual-phase *fcc* structure was not affected by heat treatment for 3 h at up to 1100 °C, there was concern whether this might induce an instability in the alloy under certain conditions. This motivated the study by He et al. [92] where arc-melted CrFeCoNi ingots were examined after long-term annealing at 750 °C for 800 h followed by water-quenching. Their TEM analyses presented in Fig. 10 showed distinct evidence of phase instability in CrFeCoNi after prolonged annealing. Specifically, in the TEM bright field image in Fig. 10 (a), many regions with darker fringes can be seen. The insets in this figure show the diffraction patterns of the matrix (inset A), from the [001] zone axis, with a *fcc* crystalline structure, and darker fringes (inset B), where two diffraction patterns from the [011] zone axis are observed; the differences in lattice parameter between the two crystals are marked as yellow and red. The red diffraction pattern could be identified as the matrix, while the yellow one should be a new separate phase. To further understand the phase separation, the lattice parameters of the two regions were characterized. The high-resolution TEM image of the darker region is presented in Fig. 10 (b); the inset shows the corresponding fast Fourier transform (FFT) image, where it is possible to verify that the darker region has the same crystalline structure as the matrix. The lattice parameter of the darker region is 0.355 nm versus 0.366 nm measured from the diffraction pattern of the matrix. The authors reported a difference in interplanar spacing of (010) planes at different zones in the HRTEM, which they associated with a 0.01 nm difference in lattice constant between the two phases and the absence of a clear phase interface. Moreover, the dark fringes after the long anneal of CrFeCoNi was attributed to decomposition, the initial stage of phase separation. It was suggested that this composition dissolution in the 750 °C annealed CrFeCoNi is similar to what is commonly observed for clustering of GP zones in Al-Cu

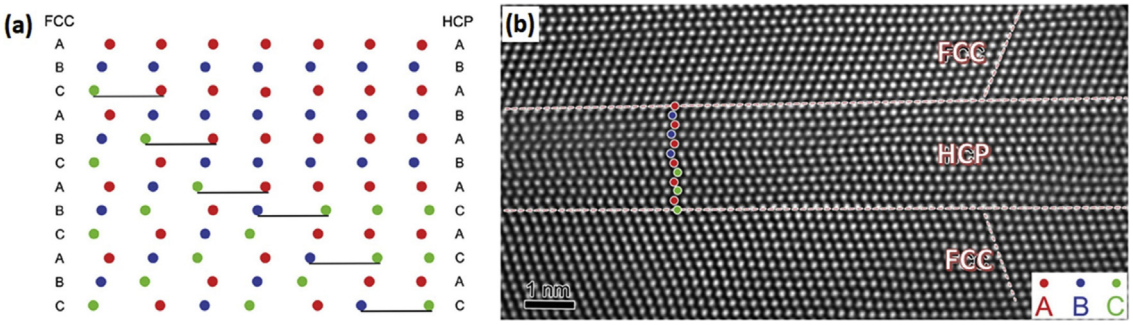

Fig. 11 – (a) Schematic illustration of the phase transformation mechanism from 12-layer ABC stacking to 6-layer ABAB and 6-layer ACAC stacking.; (b) a high-resolution STEM image illustrating 12 layers of *hcp* stacking including ABAB and ACAC sequences of a CrFeCoNi MEA deformed at extremely low temperature, −268.8 °C. Adapted from [94].

alloys. However, the long-term annealing is necessary to observe the phase separation, which can be associated with the large energy barrier or the small driving force for it to evolve to a steady-state [93].

Lin et al. [94] also investigated the phase stability of the CrFeCoNi alloy under processing and deformation conditions. In this study, the CrFeCoNi single-phase *fcc* solid solution, with an average grain size of 13 μm and compositional homogeneity, was mechanically tensile tested (at a strain rate of $\dot{\varepsilon} = 10^{-3}s^{-1}$) at 0°, −196° and −269 °C. The plastic deformation at room temperature was dominated by dislocation activity, although a small amount of deformation twins was also observed. At lower temperatures, the prominent microstructure morphologies were mainly characterized by extensive deformation twinning. Furthermore, the deformation twin thickness progressively decreased with a decrease in the deformation temperature, in spite of an increase in their total concentration. Further investigation using HRTEM indicated the formation of an *hcp* phase with the ABABAB stacking sequence and orientation relationship of $<110>_{FCC}//<11\bar{2}0>_{HCP}$ and $\{111\}_{FCC}//(0001)_{HCP}$ between the two phases. The *fcc* structure with the ABCABC stacking sequence can be transformed into an *hcp* structure with the AB stacking sequence by the glide of Shockley partial dislocations. Figure 11 (a) illustrates how the glide of one Shockley partial on adjacent {111} planes causes the stacking sequence of the subsequent *hcp* lattice to change, leading to the coexistence of two kinds of *hcp* stacking sequences. Figure 11 (b) shows a TEM image of this mechanism in the CrFeCoNi alloy deformed at −269 °C. Due to the nature of *fcc* and *hcp* lattices, the *hcp* structure can be readily transformed locally from the *fcc* structure by introducing stacking faults [95,96]. Therefore, it is clear that the stacking-fault energy (SFE) of materials, which can be understood as the energy associated with the separation between two partial dislocations [97], plays a significant role in the *fcc* → *hcp* transformation as a very small or negative SFE will favor this phenomenon. The SFE of the CrFeCoNi MEA has been confirmed both experimentally and theoretically to be around 20–25 mJ/m^2 [98–100]; alloys with such a low SFE are thus prone to display this transformation-induced plasticity (TRIP) effect.

The ternary Cantor-derived MEAs FeCoNi and CrFeNi were reported to exhibit a SFE of ~31 and ~60 mJ/m^2 respectively [98,101]. Nevertheless, the CrCoNi is the most promising Cantor-derived alloy in terms of its low SFE. The SFE for this alloy was found to be 18 ± 4 mJ/m^2 [102,103], even though negative values in the range from −48 up to −24 mJ/m^2 have been predicted for this alloy [99]. Consequently, this is the most susceptible Cantor-derived alloy to exhibit a polymorphic (*fcc* + *hcp*) structure [37]. Indeed, Ma et al. [104] established the high-strain-rate response of the CrCoNi alloy in Hopkinson-bar experiments. An excellent combination of high dynamic shear yield strength as well as large uniform dynamic shear were observed to be related with different phenomena such as high density of multiple twins, stacking faults, Lomer-Cottrell locks, and *hcp* phase transformation inside the grains of CrCoNi alloy. The evidence for these phenomena was obtained by HRTEM, as shown in Fig. 12 (a) – (d).

Indeed, the stacking-fault energy (SFE) has a profound effect on dislocation evolution, plastic deformation, and affects deformation twinning as well as phase transformations in alloys. Thus, the strain hardening of *fcc* metals is to a large extent determined by the SFE Lomer-Cottrell locks, shown in Fig. 12 (a), that are formed in the grain interior due to the reaction of leading partials from two different slip planes; as these are sessile dislocations, they can stabilize dislocation networks and as such effectively contribute to the effectiveness of strain hardening from their capability to accumulate dislocations [105,106]. Moreover, in Fig. 12 (b), one may notice nano-twinning creating a hierarchical twin network; the twin boundaries are barriers to dislocation motion, thus enhancing strength, while both full and partial dislocations can move easily along the boundaries and provide ductility [37,107,108]. As for the numerous stacking faults seen on multiple {111} planes in the grain interior, also observed in Fig. 12 (b), it is known that they also contribute to the strain hardening of the alloy but to a lesser degree than other mechanisms. The high density of stacking faults can act as barriers to dislocation motion, accumulating dislocations around them [109]. However, it is well recognized that some of these mechanisms will contribute more than others. As for the phase transition (Fig. 12 (c) and (d)) they reported a TRIP effect from *fcc* to a lamellar *hcp* phase at higher strain levels. It was suggested that this transformation is occasionally observed due to the

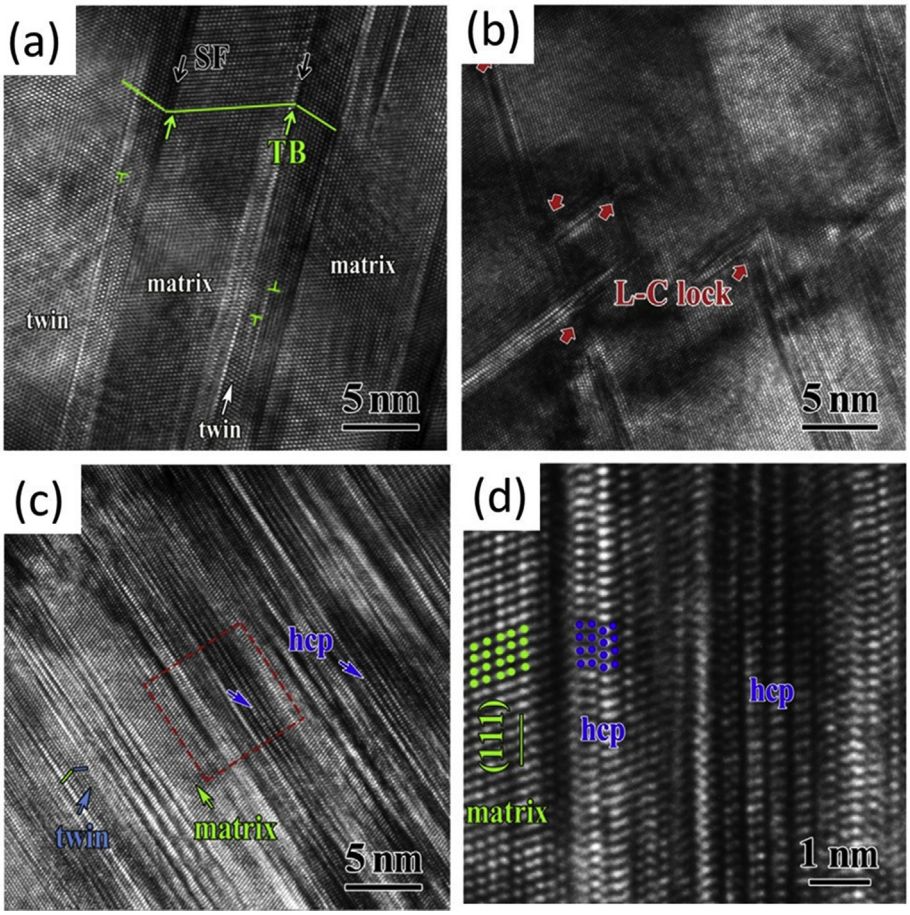

Fig. 12 – HREM images of the homogeneous shear deformation zone for the experiments conducted at cryogenic temperature in a CrCoNi MEA: (a) twin boundaries (TBs), stacking faults (SFs) and dislocations at TBs; (b) Lomer-Cottrell (L–C) locks; (c) high density of SFs and phase transformation to form *hcp* phase; (d) close-up view of the rectangle area in (c) showing this *hcp* phase. Adapted from [104].

successive formation and the overlapping of stacking faults at every other {111} plane, which was shown to occur not only for the CrCoNi alloy, but also to other alloys under large strain levels [110–112].

2.2.3. *Computer simulation and the development of HEAs*

There is a growing use of simulations aimed at accelerating development of new materials. Green et al. [113] named it the Materials Genome Initiative, defined as an effort to introduce new materials into the market faster and at lower cost, by means of computational simulation, experimental database development, and modeling. The mindset from experiment-oriented research using the trial-and-error strategy toward the simulation approach will hopefully accelerate not only the speed of discovery, but also development, production, and applications of new materials [114,115]. It is well-known that material simulation is widely used to predict properties and microstructure, by modeling materials at different scales and their characteristics in a qualitative and increasingly quantitative manner. Zhang et al. [16] suggested that multi-component alloys are good candidate materials that can benefit from this approach for rapid development in the coming years. Several calculation methods have been used to better understand multi-components alloys, such as phase diagram calculation (CALPHAD) [116,117], first-principles density functional theory (DFT) [81,118–121], and molecular dynamics (MD) [122–125].

In one of the first uses of the CALPHAD approach for the calculation of phase-diagrams, Durga et al. [126] predicted the stable phases, their relative amounts, and compositions in the quaternary equiatomic Cantor-derived MEAs. They reported that none of these alloys was expected to be single phase, which has been experimentally shown to be wrong. In a more recent CALPHAD microstructure prediction approach, Bracq et al. [76] used the TCHEA1 database, which is a specific database dedicated to HEAs, introduced by Thermo-Calc [127], and compared the experimental with calculated microstructures for several HEAs. Among those, the CrMnFeCo and CrMnFeNi alloys, which were predicted to be multiphase, were investigated. The calculated phases for the CrMnFeNi were *fcc* + *bcc* for both annealing conditions at 1000 °C and 1100 °C for 6 days. However, experimental results revealed that for the lower annealing temperature a σ phase can be identified. The authors suggested that the long annealing time

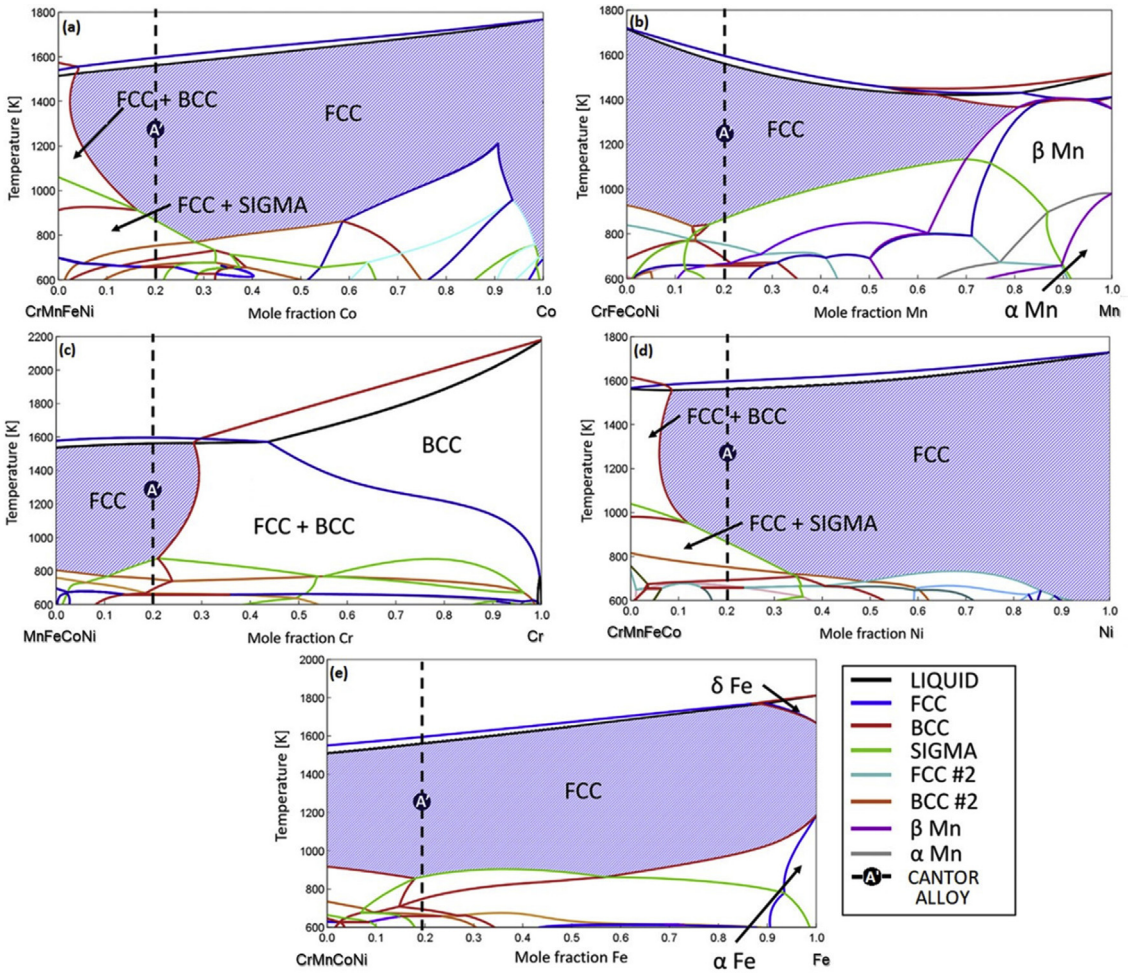

Fig. 13 – Calphad method and the TCHEA1 database for the prediction of the (a) CrMnFeNi-Co, (b) CrFeCoNi-Mn, (c) MnFeCoNi-Cr, (d) CrMnFeCo-Ni, and (e) CrMnCoNi-Fe phase diagrams. Adapted from [76].

favored the formation of the σ phase by diffusion. Indeed, the calculated phase diagram (Fig. 13 (a)) indicates that the σ phase should only be stable for this composition at temperatures below 787 °C. The same prediction was made for the CrMnFeCo alloy where it was expected to be *fcc* + *bcc* (Fig. 13 (b)), but an *fcc* + σ microstructure was observed instead. The simulation approach was right in predicting a multiphase material for these two alloys; however, the predicted phases and their amount were not consistent with experimental investigations. On the other hand, the CALPHAD + TCHEA1 predictions for the other quaternary Cantor-derived alloys, shown in Fig. 13 (c)–(e), seem to be in good agreement as a single-phase *fcc* structure was predicted. The CALPHAD method and the TCHEA1 database were shown to describe the existence domain of the *fcc* solid solution very reliably. This could lead to the conclusion that qualitative information can be drawn from this novel TCHEA1 database, as the results seem much closer to what is experimentally observed. Nevertheless, this should be evaluated carefully since the formation of some phases, such as the σ phase which can be deleterious for the properties of HEAs [55], was not shown to be easily predicted.

Thus, one should not rely solely on simulation results for determining the microstructure of either quaternary or quintenary alloys, as significant improvements in the TCHEA1 database and additional experimental work are required to increase the confidence of this tool. This is in agreement with Liu et al. [118], who discussed that although CALPHAD could be employed for compositional design, the existing databases mostly contain only binary and limited ternary alloy systems, and a reliable database for higher-order alloy systems has not as yet been established [128–130]. The bottom line here is such approaches represented by a Materials Genome approach are exceedingly useful in the prediction of ideal compositions and phase equilibria, but the properties of many of the alloys that we use today are determined by microstructure, often metastable microstructures, where such computational approaches are often found lacking. As appropriately quoted by Pickering and Jones [131]: "One can envisage that rapid approaches might dismiss most steels (had they not yet been discovered), due to their polymorphism and tendency to form brittle martensite when cooled quickly."

First-principles calculations based on Schrödinger's equation, such as Density Functional Theory (DFT) which use a set

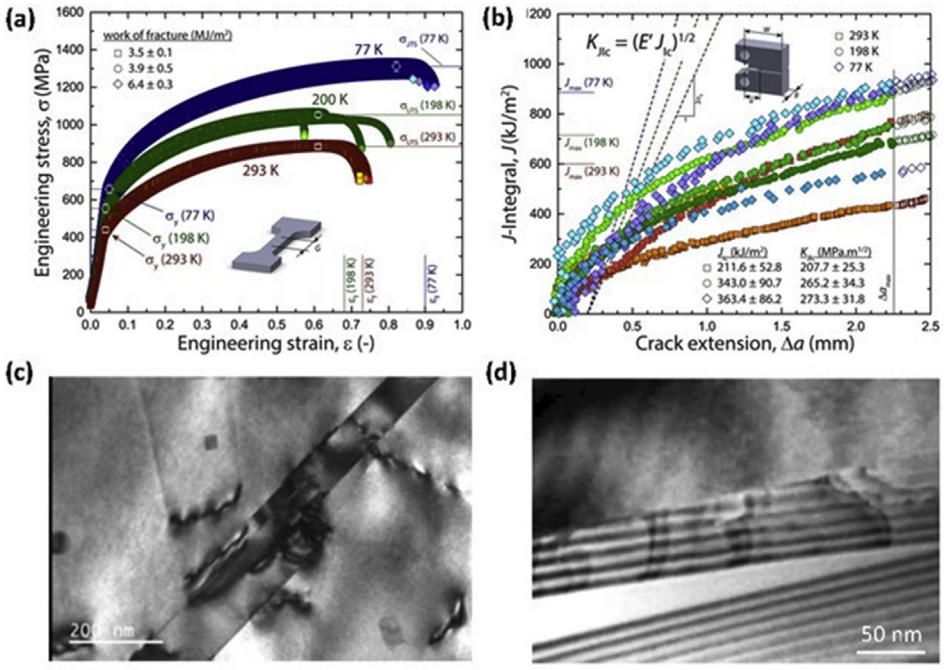

Fig. 14 – Mechanical properties of the CrCoNi alloy in the recrystallized condition (grain size of 5–50 mm). (a) Uniaxial stress-strain curves showing the progressive increase in strength and ductility at cryogenic temperatures (293 K → 77 K); (b) *J*-based resistance curves showing the corresponding increase in fracture toughness at cryogenic temperatures. Note at 77 K, the crack-initiation toughness is 273 MPa.m$^{1/2}$ and the crack-growth toughness exceeds 400 MPa.m$^{1/2}$. This alloy forms a hierarchical twin network even at room temperature. Its exceptional toughness behavior is a result of a synergy of deformation mechanisms which generate continuous strain hardening, by (c) the arrest of dislocation motion at twin boundaries to promote strength, yet (d) easy motion of dissociated dislocations along these twin boundaries to promote ductility. Adapted from [37,134].

of approximations are a valuable complement to experiments as they are accurate. But for HEAs, these calculations require the use of exceptionally large supercells to ensure the random distribution of the principal elements, demanding a huge computational capability and increasing the risk of error. Fernandez-Caballero et al. [132] used a hybrid combination of cluster expansion and Monte Carlo simulations, which are based on short-range ordering (SRO) and configuration entropy, to predict that the CrMnFeNi alloy should be a single *fcc* phase; however, this was also shown to be incorrect in experimental investigations on this alloy [75].

2.3. *Mechanical properties*

Since its discovery, the Cantor alloy has been shown to exhibit superior strength, ductility, and toughness over a wide range of temperatures [85]. One therefore should expect that the Cantor-derived MEAs might exhibit similar mechanical properties. This section accordingly discusses their mechanical properties and temperature dependence as well as the recent strategies that are being used to achieve a superior mechanical strength. It is important to mention, however, that in a recent review George et al. [21] pointed out that despite their high compositional complexity, most HEAs still lack any extensive microstructural optimization studies; this should also be considered when comparing the properties of such multiple component alloys with other traditional alloys. Indeed, we intend to address specific examples as we report and compare the mechanical properties of these MEAs alloys.

Zhu et al. [54] compared the hardness of the CrMnFeCo, CrMnFeMn, and CrMnFeCoNi alloys; both quaternary alloys were shown to be multiphase. The CrMnFeCo alloy exhibited a hardness almost four times higher than CrMnFeNi. This is possibly associated with the precipitation of the harder σ phase with its tetragonal structure.

Ma et al. [104] studied the dynamic deformation of CrCoNi with different grain sizes and microstructures produced by cold rolling and annealing at various temperatures. Hopkinson-bar testing revealed a combination of high dynamic shear yield strength and large uniform dynamic shear strain (prior to localization), which exceeded all other metals and alloys reported so far. The combination of several mechanisms, such as grain refinement, high density of multiple twins, stacking faults, Lomer-Cottrell locks and the transformation of the *fcc* phase into an *hcp* phase, were claimed to be responsible for the high dynamic shear properties observed.

The superior mechanical properties exhibited by these CrCoNi alloys, when compared to their "parent" Cantor alloy, were discussed by Laplanche et al. [133]. They suggested that in the early stages of plastic deformation, Shockley partials are activated on the {111} planes. Thus, the ½ <110> dislocations dissociate into 1/6 <112> dislocations. In addition, the stacking-fault energy of the CrCoNi alloy, which is about 25%

Table 2 – Properties of Cantor-derived MEAs investigated in this work in comparison to the CrMnFeCoNi HEA.

Alloy	Microstructure	Mechanical Properties							SFE (mJ/m^2)
		σ_y (MPa)	σ_{UTS} (MPa))	ε_f (%)	Hardness (HV)	K_{JIc} (MPa.m$^{1/2}$)	E (GPa)	G (GPa)	
CrMnFeCoNi	*fcc* single phase	200–350	550–650	60–80	145	217	202	80	30 ± 5
CrFeCoNi	*fcc* single phase	320	600–660	27	134–150	–	214	86	27 ± 4
CrCoNi	*fcc* single phase	430	800–880	73	198	208	235	90	18 ± 4
FeCoNi	*fcc* single phase	190	320–470	28	115–124	–	175	68	70
CrMnFeNi	multiphase	230	450	28	164	–	180	–	–
MnCoNi	*fcc* single phase	168	614	35	–	–	191	79	–
MnFeNi	*fcc* single phase	225	600	29	–	–	177	77	–
CrMnFeCo	multiphase	338	795	4.3	551	–	–	–	–
MnFeCoNi	*fcc* single phase	170	556	36	136–149	–	–	–	–
CrMnCoNi	*fcc* single phase	550	810	18	–	–	–	–	–
CrFeNi	*fcc* single phase	160	–	–	187	–	180–190	79	–
CrFeCo	multiphase	–	–	–	403	–	–	–	–
MnFeCo	multiphase	–	–	–	170	–	–	–	–
CrMnCo	multiphase	–	–	–	–	–	–	–	–
CrMnNi	multiphase	–	–	–	–	–	–	–	–
CrMnFe	–	–	–	–	–	–	–	–	–

σ_y = yield strength; σ_{UTS} = ultimate tensile strength; ε_f = strain at fracture; K_{JIc} = fracture toughness; E = elastic modulus; G = shear modulus; SFE = stacking-fault energy.

lower than the Cantor alloy, favors the formation of a hierarchical nano-twinning network. As mentioned above, twin boundaries act as barriers to dislocation motion which result in the strengthening of the alloy; however, both full and partial dislocations are capable moving fast along the boundaries, which favors the higher ductility of the CrCoNi alloy [37].

Furthermore, Gludovatz et al. [134] showed that the CrCoNi alloy displayed strength-toughness properties that exceed those of most advanced alloys such as stainless steels, nickel-based super alloys, and others HEAs. At room temperature, the alloy exhibited a tensile strength of ~1 GPa, failure strain of approximately 70% and a K_{JIc} fracture toughness above 200 MPa m$^{1/2}$; at cryogenic temperatures, the strength levels reached above 1.3 GPa and failure strains were ~90% with a K_{JIc} fracture toughness of 275 MPa m$^{1/2}$. This is shown in Fig. 14 (a) and (b) respectively in terms of the uniaxial stress-strain curves and *J*-based resistance (fracture toughness) curves of a recrystallized CrCoNi alloy at temperatures between 0 °C down to −196 °C [134]. It is somewhat remarkable that such excellent strength, ductility and toughness, which ranks among the best of any material, is achieved in a simple single-phase equiaxed grain structure. The exceptional fracture toughness, however, is simply a consequence of the deformation mechanics in these alloys which have high lattice friction yet a low SFE. This enables them to develop a sequence of deformation mechanisms under increasing strain which provides a continuous source of strain hardening [37]; this obviously increases the strength but simultaneously increases the tensile ductility by delaying any necking instabilities. Accordingly, these alloys do not display any strength/ductility trade-off as they can generate deformation mechanisms that promote strength, such as dislocation arrest at grain and twin boundaries (Fig. 14 (c)), yet these same twin boundaries can provide pathways for the motion of dislocations to promote ductility (Fig. 14 (d)) [37]. This is further enhanced at decreasing temperatures by the preponderance of deformation twinning and the TRIP phenomenon to form the *hcp* epsilon martensite phase (although the latter mechanism in excess can eventually degrade the toughness of the alloy; the transformation-induced deformation creates more strain hardening, but the resultant epsilon martensite product phase is quite brittle).

Table 2 summarizes several properties reported so far for the Cantor derived MEAs as well as the CrMnFeCoNi alloy.

2.3.1. *Temperature dependence*

The influence of a wide range of temperatures on the yield strength, ultimate tensile strength, and uniform elongation of several Cantor-derived MEAs was addressed by Wu et al. [72]. Figure 15 summarizes these properties. The strength decreases with the increase of temperature and, consequently, the maximum values are observed at cryogenic temperature. Gludovatz et al. [134] pointed out the non-linearity between solid-solution hardening and increased number of main elements, as higher values were attained for the ternary CrCoNi MEAs. This indicates that not only the number of main elements, but also the type of added elements plays a major role in the strength of these alloys as it may be observed for the Cr-containing alloys.

Tsai et al. [135] reported serration behavior on the stress-strain curves, *i.e.*, the Portevin-Le Chatelier effect, for the FeCoNi and CrFeCoNi as well as CrMnFeCoNi, alloys in uniaxial tensile tests at strain rates from 10^{-5} to 10^{-2} s^{-1} and temperature range from room temperature up to 700 °C. Unlike the traditional Portevin-Le Chatelier effect, where the interstitial atoms play a crucial role, local dislocation-core diffusion of substitutional solutes was proposed to be responsible for dislocations pinning in these alloys (Fig. 16). The higher temperature range observed for this phenomenon, above 300 °C, is corroborated by the rearrangement of solute atoms at or near the dislocation cores.

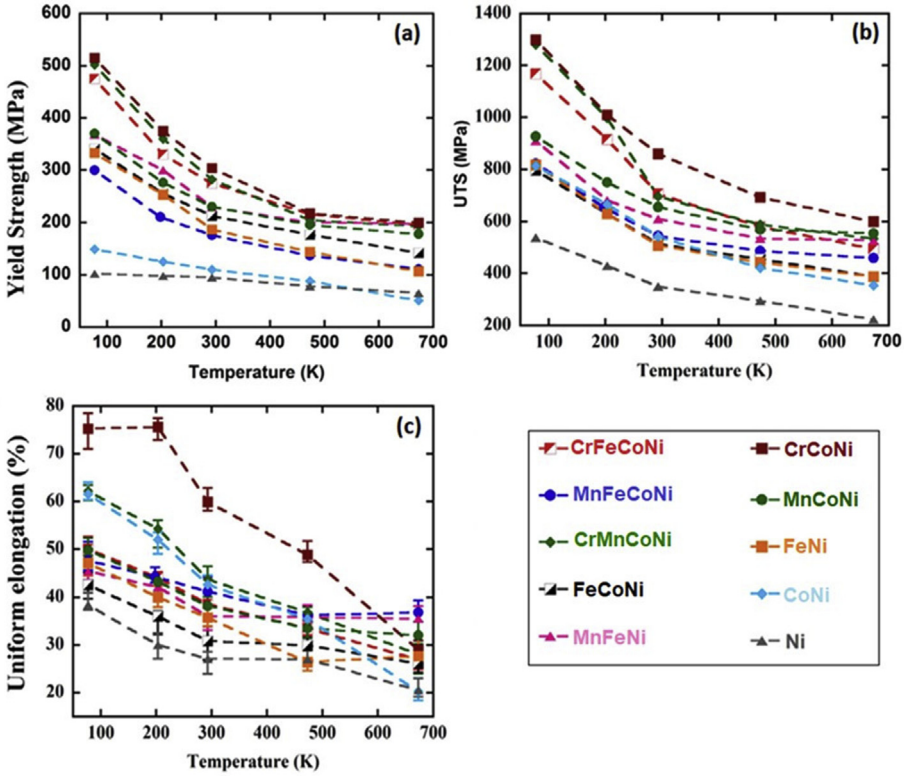

Fig. 15 – Temperature dependence of the mechanical properties of different variants of the CrMnFeCoNi alloy: (a) 0.2% offset yield stress, (b) UTS, and (c) uniform elongation to fracture. Adapted from [72].

2.3.2. *High strain-rate behavior*

Understanding the plastic deformation processes in HEA and MEAs as the strain rates are increased from quasi-static to high is considered critical for the structural application of such materials [136]. Sharma et al. [137] discussed that the knowledge of high-strain deformation is fundamental for applications where strain rates higher than ~10^2 s^{-1} are encountered, which includes lightweight armor materials, blast impact of debris on aircraft panels, satellites, or spacecraft, as well as high-speed machining, all of which might be seen as relevant opportunities for the use of MEAs and HEAs. As discussed in the previous section, the deformation behavior in Cantor-derived MEAs under quasi-static loading at strain-rates as low as 10^{-2} to 10^{-4} s^{-1} reveals the predominant contributions of slip and twinning mechanisms [134,138,139]. Understanding the deformation behavior at strain rates higher than 10^2 s^{-1} is a complex task due to the localized strain accumulating along the adiabatic shear bands [140]. In this context, Li et al. [112,141] were the first to examine the dynamic mechanical behavior and shear localization of the $Al_{0.3}$CoCrFeNi and CrMnFeCoNi HEAs. They reported that the high strain-hardening ability, enabled by solid-solution hardening, forest dislocation hardening and twinning hardening, the high strain-rate sensitivity and modest thermal softening of the $Al_{0.3}$CoCrFeNi HEA all contributed to the high resistance to shear localization. They also observed for the Cantor alloy that the same combination of the excellent strain-hardening ability and general thermal-softening effect gives rise to remarkable resistance to shear localization. Similar to the $Al_{0.3}$CoCrFeNi HEA, the high strain-hardening rate was attributed to solid-solution hardening, cutting forest dislocations, and twinning hardening. Further investigations using a split Hopkinson pressure bar were performed on a CrFeNi MEA by Fu et al. [142]; they disclosed the outstanding strain-hardening of the alloy and strain-rate sensitivity (SRS), which caused the appearance of adiabatic shear bands only for shear deformations of ~14.5; an enhancement in the yield stress to over 1300 MPa in comparison to the 667 MPa under quasi-static conditions, was also measured. They also observed that microvoids preferentially nucleate in the core areas of the shear band where the localized strain is concentrated, and where the temperature is high. These microvoids form microcracks as the shear strain increases; finally, the microcracks evolve into a regional crack which leads to the rapid fracture of the shear band. CrCoNi [143] and CrFeCoNi [144] were some other Cantor-derived MEAs investigated using the Split-Hopkinson bar experiment approach.

Shabani et al. [145] investigated the dynamic behavior of CrFeCoNi at tensile $\dot{\varepsilon} = 10^2$ to $10^3 s^{-1}$, using a modified Hopkinson bar. They observed that the dominant deformation mechanism shifted from dislocation slip at lower strain rates to the addition of deformation by nano-twinning at high strain rates. The strain-rate sensitivity of the flow stress (SRS) was found to be equal to 0.048. The positive value of SRS suggests that the mechanical properties might be improved

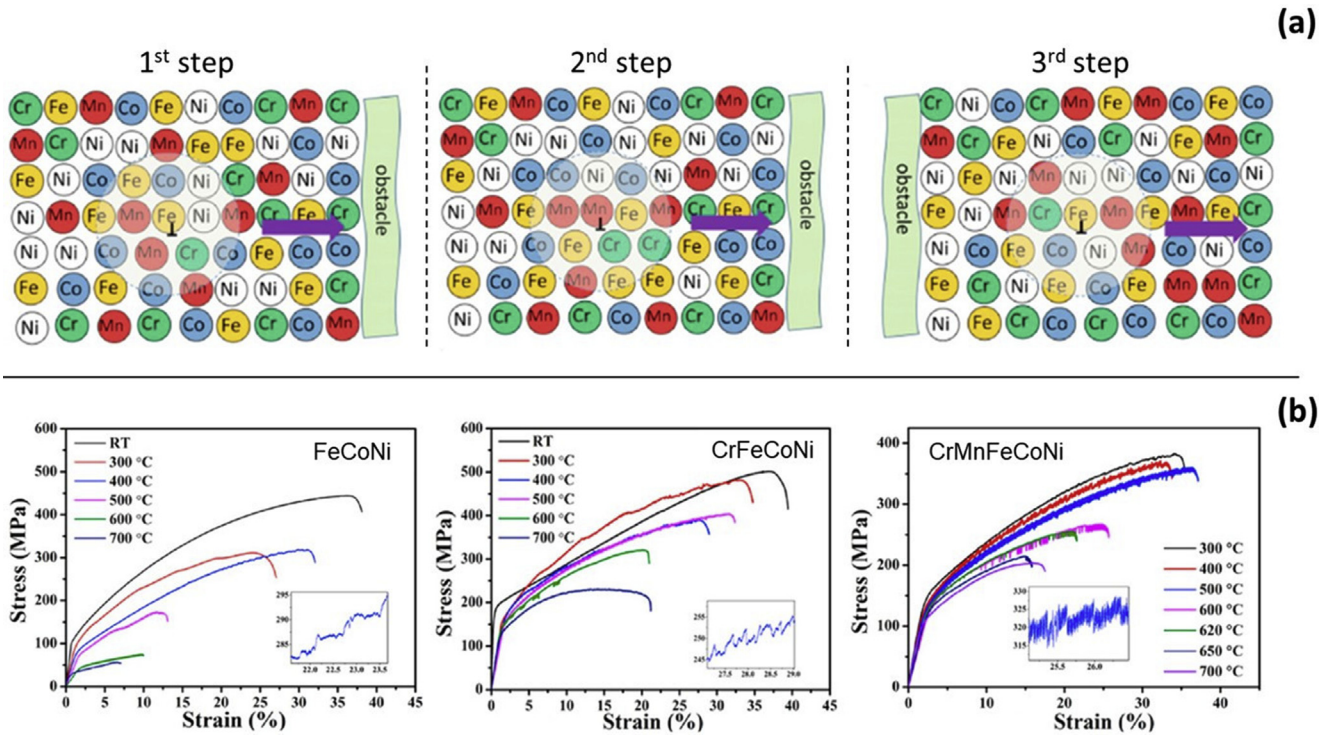

Fig. 16 – Schematic illustration showing different stages of atomic configurations for pinning during the dislocation motion in the CrMnFeCoNi alloy by the following mechanism; if the solute atoms in the dashed circle represent the dislocation core: 1st step: the dislocation encounters an obstacle; 2nd step: solute atoms at the dislocation core rearrange *in situ* to a lower the strain-energy level and thus pin the dislocation; 3rd step: the new position of the dislocation after being released from its atmosphere and then overcoming the obstacle under an increased stress. (b) Stress-strain curves obtained from tensile testing at the strain rate of 10^{-4}/s of FeCoNi, CrFeCoNi and CrMnFeCoNi. Adapted from [135].

with increase in the strain rate. A high SRS could be associated with the distorted lattice of this alloy as well as with thermally activated mechanisms [146,147]. These findings were corroborated by Gao et al. [148], who in addition to split-Hopkinson experiments in tension used an artificial neural network simulation to validate their results.

Recently, it was shown that under certain conditions, high-strain rates can lead to amorphization in shear bands that arise during deformation. Zhao et al. [149] subjected an equiatomic CrMnFeCoNi to severe plastic deformation to investigate the subsequent modes of shear dynamic deformation. They observed a dense structure which included stacking faults, twins, and *fcc* → *hcp* phase transformation, as well as islands of amorphous material. Amorphization was proposed as a final stage of a sequence of sequential deformation mechanisms for the Cantor alloy subjected to increasing degrees of deformation. As many of these phenomena under high strain rate have been associated with the stacking-fault energy [150,151], it could be possible that alloys such as CrCoNi or CrFeCoNi that display a lower stacking-fault energy compared to the Cantor alloy (see Table 2) may also exhibit amorphization bands under certain conditions. In fact, recently Jian et al. [152] performed molecular dynamics simulations to investigate shock-induced amorphization in a CrCoNi MEA. They showed that, at lower shock velocities (U_p = 800 m/s), no amorphization occurred, and mechanisms of dislocation slip and twinning dominate the plastic deformation of the alloy. However, with the increase in the shock velocity (U_p = 1000–1200 m/s), solid-state amorphization became appreciable, whereas at ultra-high shock velocities (U_p = 1400 m/s), extensive amorphization occurred, such that by the end of the compression stage over 30% of the material exhibited an amorphous structure.

2.3.3. *Strategies to improve the mechanical properties of cantor-derived MEAs*

In addition to the remarkable microstructure and mechanical properties exhibited by the Cantor-derived MEAs shown in the previous sections, several other strategies have been investigated in recent years in order to achieve superior properties. Tsai et al. [153] proposed that the multicomponent alloys entered a different stage of development, where they are usually designed to meet certain goals. Researchers have carefully chosen components, deliberately introduced multiple phases, and tailored microstructures. Here we discuss such different strategies that have been used for Cantor-derived MEAs, although in certain cases, this has resulted in the shift from the equiatomic composition of these alloys. However, modifications in the composition of an alloy, such as adding interstitial elements and/or precipitating second phases, can be a way to overcome the trade-off in strength and ductility in certain equiatomic alloys [18,154–157].

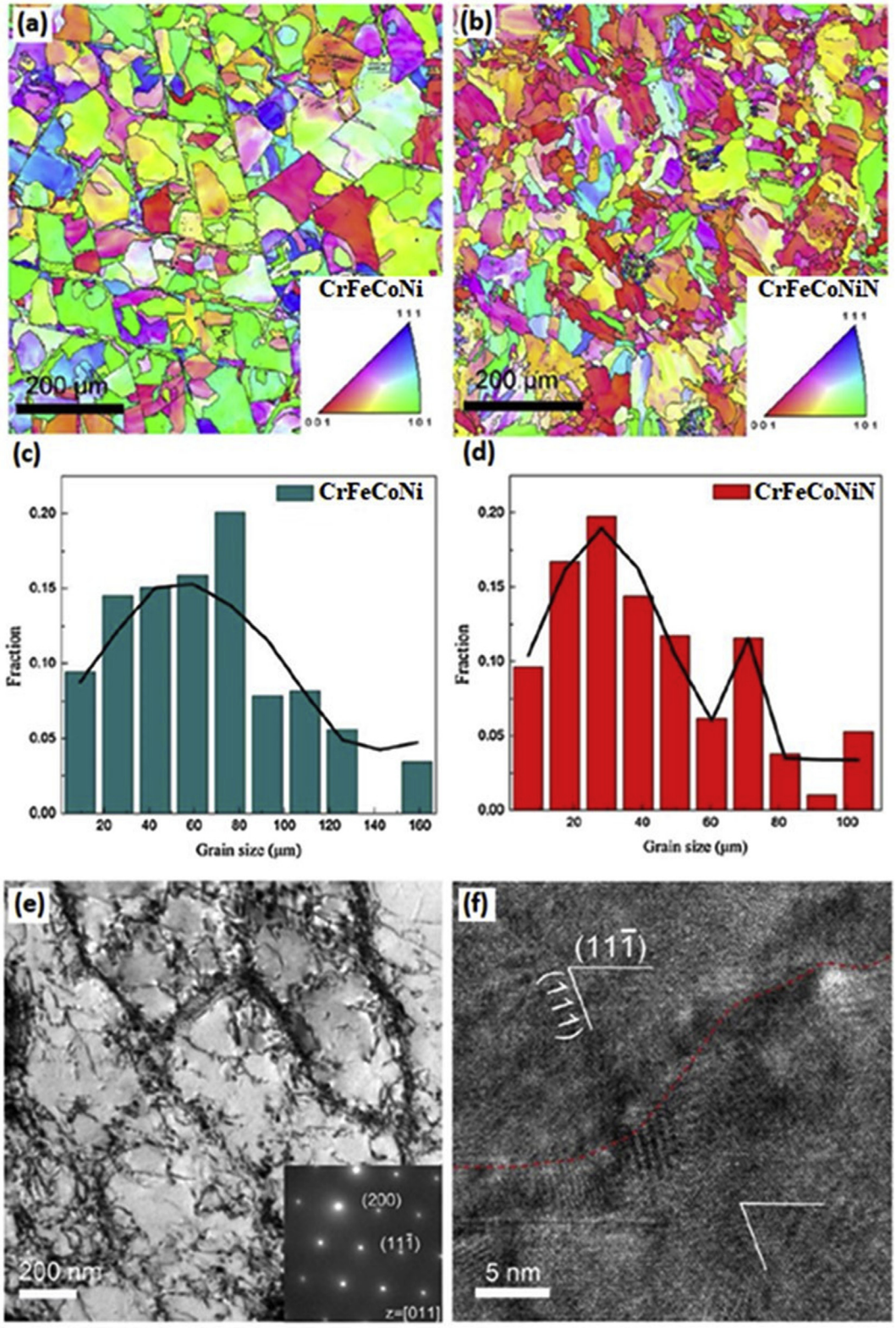

Fig. 17 – Microstructures of the additively manufactured HEAs (a, b) EBSD maps of undoped and N-doped CrFeCoNi, respectively (c, d) Grain size distribution of the undoped and N-doped HEA, respectively. (e) TEM image showing the dislocation networks at high magnification; the inset pattern confirms the single-phase *fcc* structure of the N-doped HEA. (f) High-resolution TEM image showing the wall structure of dislocation networks in the N-doped alloy. Adapted from [160].

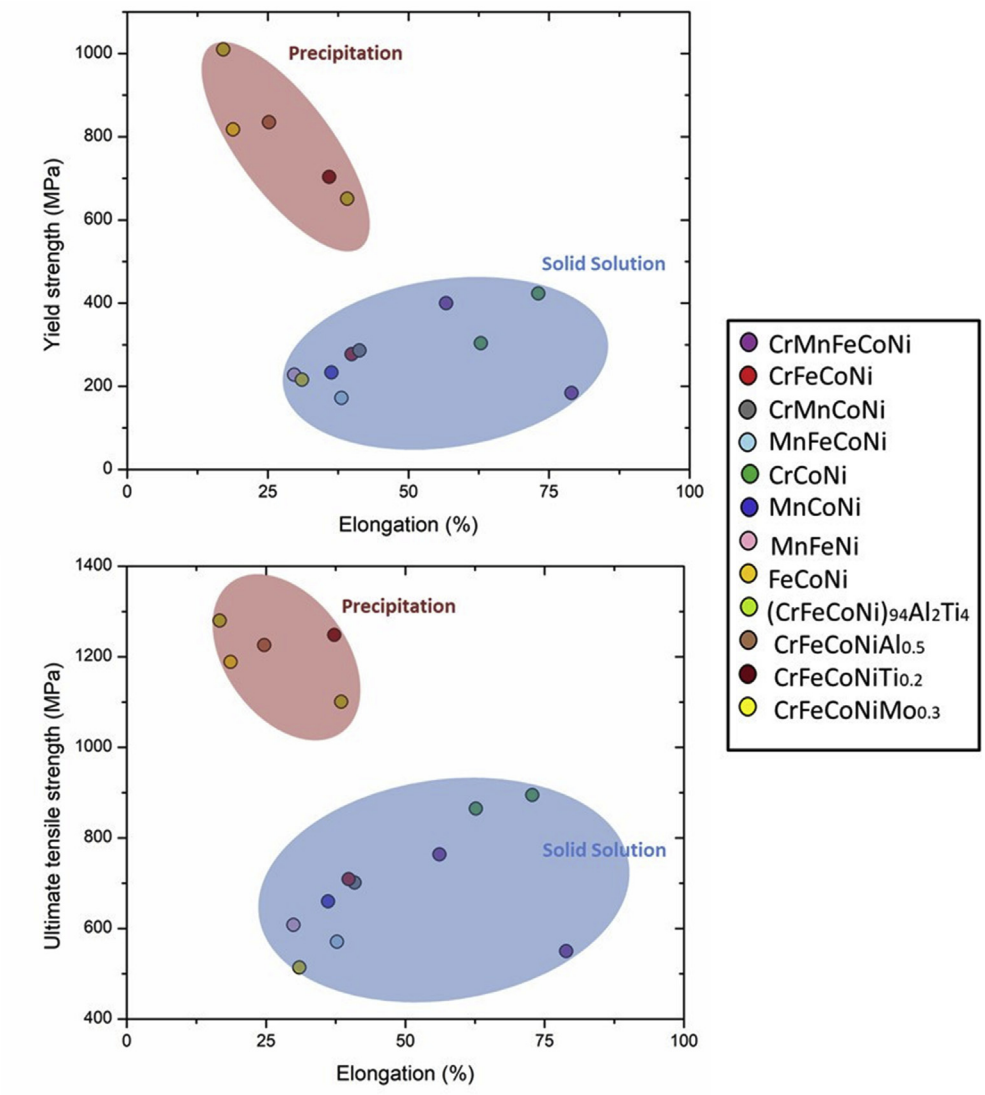

Fig. 18 – Influence of the strengthening mechanism – precipitation strengthening *vs.* solid-solution hardening – on the yield strength and ultimate tensile strength of various medium- and high-entropy alloys.

2.3.3.1. *Solid-solution strengthening*. One issue with the CrCoNi-based alloys is that, although they strain harden very effectively, they often display a relatively low yield strength. To counter this, the effect of interstitial atoms such as boron, nitrogen, and carbon has been evaluated in some of Cantor-derived MEAs in part to provide a source of initial hardening [158–161]. Song et al. [160] claimed to overcome the strength-ductility trade-off in CrFeCoNi alloys with and without N-doping. They reported that the undoped alloy displayed a yield strength of 520 MPa and a good tensile elongation of 27%. However, the N-doped alloy exhibits a much higher yield strength of ~650 MPa. Doping other HEAs with interstitial atoms can strengthen these alloys without diminishing ductility [162,163]. Surprisingly, the N-doped CrFeCoNi alloy undergoes an increase in the tensile elongation up to 34%. This can be reasoned to be associated with its complex heterogeneous hierarchical microstructure with the interstitial nitrogen giving rise to a bimodal grain structure with low angle boundaries, and dislocation networks (Fig. 17).

The effect of carbon and silicon additions was investigated by Yang et al. in a CrMnFeCo alloy [161]. They verified that C- and Si-doping were responsible for an enhancement of the alloy's structural stability due to an increase in the SFE but also for modifying the deformation mechanism from dislocation slip to twinning under increasing strain. On the other hand, Liu et al. [164] showed that C-doping of a CrFeCoNi alloy could lead interdendritic segregation of Cr and C, resulting in grain-boundary precipitation of $M_{23}C_6$ carbides as well as grain refinement. It is clear that adding interstitial atoms such as C or B enhances strengthening; however, these atoms have been reasoned to activate other strengthening mechanisms and could be used to induce SRO to further enhance the mechanical properties of these alloys [165].

Substitutional solid-solution strengthening is also commonly found in Cantor-derived MEAs, especially the CrFeCoNi alloy. Liu et al. [166] investigated the mechanical behavior of $CrFeCoNiMo_x$ ($0.1 < x < 0.3$). They observed that lower amounts of Mo did not result in the precipitation of

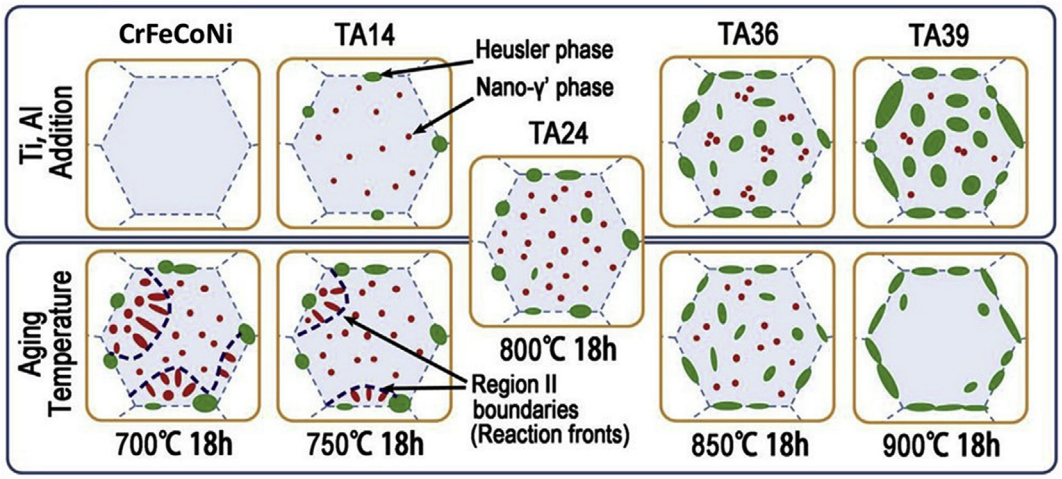

Fig. 19 – Schematic illustrations showing the effect of Ti and Al additions, as well as the aging conditions, associated with the precipitate distribution and evolution in the CrFeCoNi MEA. Adapted from [193].

second phases and the alloy was characterized to be *fcc*; however, the Mo additions even in atomic concentrations as low as 2.44 at.% were able to produce an increase of both the yield strength and tensile strength without compromising the ductility of the alloy, in comparison with the CrFeCoNi MEA. In contrast, Wang et al. [167], found that the addition of 2.4 at.% of Al did not lead to a substantial increase in the hardness, as both CrFeCoNi and $Al_{0.1}$CrFeCoNi alloys exhibited Vickers hardness of ~120 HV. Du et al. [168] showed that adding a Cu concentration lower than 5 at.%, the Cu atom dissolved in the *fcc* matrix. As the concentration of Cu was increased, it provided a solid-solution strengthening effect in the *fcc* matrix, since its atomic radius is larger. When the Cu concentration was increased to ~3 at.%, the elongation decreased 31% while the YS and UTS were increased. The solid-solution hardening for other substitutional elements has also been investigated for these alloys, including: Ti [169,170], Mn [171,172], V [173,174], and Nb [175–177].

Despite these experimental results, determining the precise contribution of solid-solution strengthening in MPEAs is still considered a challenge as the idea of "solute" and "solvent" lose their conventional meaning [42]. However, when considering Cr, Fe, Co and Ni, they present similarities regarding their atomic sizes and a nearly equal to zero mixing enthalpies of different atom-pair of these four elements. Therefore, when incorporating in the CrFeCoNi matrix substitutional elements, in concentrations as low as 5 at.%, of an atom that clearly differs from the matrix, such as Mo, a standard model for substitutional solid-solution strengthening based on dislocation-solute elastic interaction can be used to assess the contribution of solution strengthening associated with the substitutional element [178]. Varvenne et al. [179] proposed a general theory for the solid-solution strengthening of *fcc* HEAs. They suggested that strengthening is achieved, mainly, due to dislocation interactions with the random local concentration fluctuations around the average composition, even though such fluctuations may be difficult to measure. Their work also contributed for understanding relevant points regarding the strengthening of these alloys including the influence of the: number of elements main elements, equiatomic compositions, stacking-fault energy, and shear modulus.

2.3.3.2. *Second phase/precipitation strengthening*. Precipitates formed during material processing are a good way to synchronously improve the strength and often ductility of Cantor-derived MEAs [88,180,181]. The controlled precipitation of second phases in single-phase *fcc* MEAs that exhibit outstanding ductility but low strength for certain practical applications has been considered as a promising strategy to produce alloys with superior properties [182]. With this scenario, the CrFeCoNi is the preferred Cantor-derived MEA to be used as base metal (matrix) although some research using other Cantor-derived MEAs as matrix can also be found [102,183]. Figure 18 presents the effect on the room temperature yield strength, ultimate tensile strength, and elongation achieved in the CrFeCoNi alloy by the precipitation of different second phases.

Precipitation strengthening by introducing dispersed hard $L1_2$-structured gamma prime (γ') particles into the CrFeCoNi *fcc* matrix (γ phase) has been recently reported [169,184–186]. This type of strengthening mechanism may be favored by the CrFeCoNi matrix as Co is known to be a stabilizer of γ' while Fe and Cr can improve the ductility of the γ' phase [187,188]. Zheng et al. [184] doped the CrFeCoNi matrix with Al (in Ni:Al ratio = 3:1) to produce Ni_3Al as strengthening phase. Similarly, Han et al. [185] elected to use Ti as an addition as this would give rise to Ni_3Ti γ' precipitates. One dubious aspect is that both precipitates can hinder twin nucleation and growth in the CrFeCoNi alloy [169]. The influence of coherent precipitates on twinning in conventional Ni- and Mg-based alloys has been previously examined, but no conclusive answers were obtained [189–191]. Yang et al. [192] suggested that twinning rarely occurs in FeCoNi-based MEAs strengthened by coherent γ' precipitates. They showed that stacking faults would prevail rather than twins when the alloy is deformed at

cryogenic temperatures, and that the γ′ precipitate might hinder the formation of twins. However, Tong et al. [169] found microtwins in a precipitation-strengthened $CrFeCoNiTi_{0.2}$ when such an alloy is deformed at −196 °C; it was proposed that the chemical ordering of γ′ particles might markedly increase the energy barrier for twin nucleation.

He et al. [193] simultaneously doped the CrFeCoNi-matrix with Al and Ti. They observed that two types of precipitates were formed for different aging times and temperatures, ranging from 0.5 to 48 h and at 700 °C up to 900 °C respectively. Nanosized, coherent $L1_2$-Ni_3(Ti, Al) precipitates and $L2_1$-$(Ni, Co)_2TiAl$ Heusler phase were formed and found to contribute to strengthening. However, the brittle Heusler particles were also considered as the primary cause for the loss in ductility shown by this alloy. The volume fraction of Ni_3(Ti, Al)-type precipitates can be increased with increasing Ti and Al additions, but excessive additions of these two elements also promotes the formation of brittle micrometer-sized $(Ni, Co)_2$-TiAl Heusler phase, which significantly compromises the alloy's tensile ductility. Figure 19 presents a schematic illustration of the evolution of the precipitates in terms of the degree of Al and Ti additions as well as the aging conditions.

Other precipitate-forming elements added to improve the yield strength of the CrFeCoNi-matrix are Mo, Nb, and Cu [166,194–198]. Mo-doping resulted in the precipitation of extremely hard topologically close-packed phases (*tcp*) such as μ and σ, as observed by Liu et al. [166]. Although brittle, these intermetallic phases are known to exhibit hardness values up to 15 GPa [199]. On the other hand, the addition of Nb as a precipitating element resulted in a Laves phase imbedded in the *fcc* matrix. With the increase in Nb-doping, the volume fraction of the hard and highly brittle Laves phase increased, leading to a marked decline in ductility [197]. However, it was shown that in compression the strength of this could reach 2.5 GPa with an associated fracture strain of ~28%.

2.3.3.3. *Grain-boundary strengthening*. We have described so far how the addition of new elements can be utilized as an important strategy to enhance, or at least influence, the mechanical properties of the Cantor-derived MEAs. However, tailoring of the microstructure may be another way of improving the mechanical properties of these alloys [200–202]. In this scenario, grain refinement is an important mechanism for the strengthening of metallic alloys, as the grain boundaries act as strong obstacles to dislocation motion [97]. Severe plastic deformation is one of the most powerful techniques to achieve ultrafine-grained or even nanocrystalline materials; this has been successfully applied in medium- and high-entropy alloys, especially through the use of high-pressure torsion (HPT) [203–209].

Gubicza et al. [207] investigated the microstructure and hardness evolution of a CrFeCoNi alloy processed by an HPT technique and compared the results with those obtained for the Cantor alloy processed under the same conditions. The authors found out that up to 20 turns of HPT at room temperature introduced a high shear strain that resulted in a saturation grain size of ~80 ± 10 nm. The observed shear strain was found to be almost three times higher than that observed for the Cantor alloy, although the saturation hardness was almost the same for both alloys, i.e., ~5.1 GPa, which they associated with the close values of twin fault probability exhibited by these alloys. Yoshida et al. [208] produced HPT-processed samples of CrCoNi with grain sizes varying from 100-500 μm to 200–300 nm, in order to assess the friction stress and Hall-Petch relationship in this alloy. They clarified that the friction stress of this alloy was much higher than conventional *fcc* pure metals and even the Cantor alloy, which they attributed to the fluctuation in the Peierls potential for dislocation motion.

Gigax et al. [75] used a different severe plastic deformation (SPD) technique to produce an ultrafine grained CrMnFeNi alloy. Significant refinement of the grain size was observed for all processing conditions, with an average obtained grain size as low as 95 nm compared to 232 μm for the reference condition. This resulted in a substantial increase in hardness (up to 4.9 GPa), a tensile yield strength (up to 780 MPa), and ultimate tensile strength (up to 810 MPa) against ~2.8 GPa, 230 MPa, and 450 MPa for the unprocessed condition, respectively. However, all the SPD conditions exhibited a major deterioration in ductility, from about 28% to only 1.45%. Indeed, this is a universal characteristic of metals subjected to SPD. The drastic decrease of ductility is primarily due to the decrease in work hardening. The small grains provide dislocation sinks and their density does not increase with strain. Thus, tensile instability sets in right away.

2.3.3.4. *Heterogeneous grain structure*. A drawback of many nanocrystalline materials is the aforementioned lack of sufficient ductility. An interesting way to overcome this problem and obtain a superior strength-ductility synergy was obtained in CrCoNi alloys [210,211]. Lu et al. [210] produced several homogeneous and heterogeneous grain structures through heavy deformation and subsequent annealing treatment. They showed that the heavily deformed alloy, cold-rolled 90%, exhibited an excellent yield strength of ~1.6 GPa, but with a poor ductility of ~3%. The fully recrystallized structure followed the Hall-Petch relationship, as observed previously by Yoshida et al. [208] and shown in Fig. 20. However, the

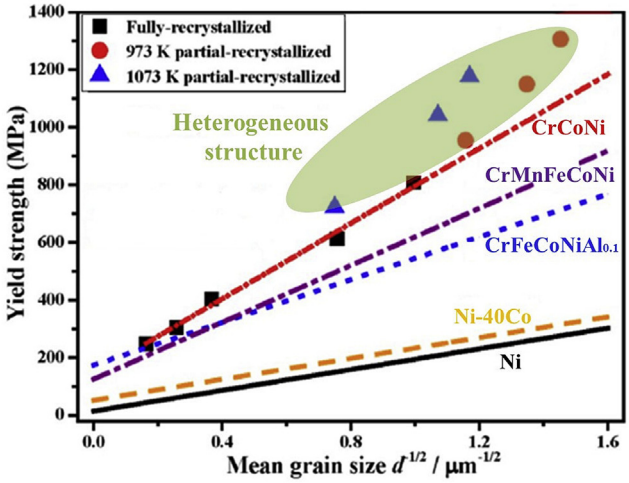

Fig. 20 – Variation in the yield strength as a function of the mean grain size in the CrCoNi MEA, showing a comparison of the Hall-Petch relationship for a series of different *fcc* alloys. Adapted from [210].

partially recrystallized anneal resulted in a microstructure abundant in recrystallization twins and multiple grain sizes, which enhanced both strength and ductility; this is also presented in Fig. 20. The superb strength-ductility synergy observed in the heterogeneous structure compared to a nanograined and/or ultrafine-grained structure can be explained in terms of the high density of geometrically necessary dislocations that are generated to accommodate the strain gradient that results from the incompatibility of hard and soft domains in the heterogeneous structure [212,213]. Wu and Zhu [214] showed that in heterogeneous materials, the plastic strain gradient results in a back stress due to the pileup of dislocations in the interface of these soft and hard domains; this results in back stress-induced hardening during tensile deformation. Similarly, this effect has been shown to effectively hinder necking, thus improving the uniform ductility, during tensile testing of dual-phase steels [215–217]. Yang et al. [211] pointed out that despite the CrCoNi alloy being a single-phase *fcc* alloy, the same mechanism that is observed in dual-phase steels would occur. They specifically discuss the predominant role of low stacking-fault energy, which favors the formation of twins during recrystallization as well as deformation twins and stacking faults during tensile straining, that combine results in this microstructural heterogeneity and superb strength-ductility relationship.

3. Final remarks

Extensive work involving experimental, theoretical and simulation studies, has been performed, in particular over the past decade, to explore the composition, microstructure, phase stability and mechanical behavior of high-entropy alloys and other multiple principal element materials. Indeed, this has become one of the dominant fields of metallurgy with continuous development and discoveries that must be understood and explored in depth. In this brief review, we have examined such research specifically with respect to the medium-entropy alloys derived from the original CrMnFeCoNi Cantor alloy, as this has been a particularly active topic for both experimental and atomic simulation studies. However, there are still many issues with these MEAs that warrant significant further investigation. To conclude this review, we briefly describe some of these topics.

(1) Theoretical studies relating to the microstructure/mechanical property relationships still need to be further explored. In particular the serration behavior on stress-strain curves in these alloys should be intensively studied and understood. The fact that such serrations are often reported at liquid helium temperatures but not at 77 K (liquid nitrogen temperatures), and whether they are mechanically- or thermally-induced, has still not been fully explained. The investigation of the tension versus compression behavior over a wide range of strain rates and temperatures is also still incomplete. Massive twinning could be a possible cause. These topics speak to the vital question of the nature and sequence of the deformation mechanisms in these alloys, which are the fundamental key to underlying their strength, ductility and toughness properties, all of which are essential if MEAs are to be seriously considered for future industrial structural applications.

(2) Among the 15 equiatomic Cantor-derived MEAs, the ternary CrCoNi and quaternary CrFeCoNi are those that have exhibited the most remarkable properties. Indeed, the strength-toughness properties of the CrCoNi exceed those reported for the vast majority of important engineering materials, including their "parent," the Cantor alloy. The CrFeCoNi alloy displays an impressive stability of the *fcc* phase which has made it the focus of attention of many research studies aiming to overcome the strength-ductility trade-off by the addition of precipitating elements. However, this is not the only strategy to enhance the mechanical properties of the Cantor-derived MEAs as solid solution, grain refinement, and heterogeneous grain structure have been shown to have an impact on their behavior. On the other hand, there is still only sparse information of the other ternary derivatives of the Cantor alloy, specifically the CrFeCo, CrMnCo, MnFeCo, CrMnFe, and CrMnNi alloys.

(3) From a scientific perspective, there is still uncertainty concerning the existence, effect and mechanisms of local ordering in these alloys, indeed in all multiple principal element alloys which involve non-dilute solid solutions. Such ordering has been clearly demonstrated with density-functional theory and molecular dynamics Monte Carlo simulations, but these do not always accurately reflect real materials at conventional temperatures and strain rates. Although recent studies have been able to directly observe such local order in certain CrCoNi-based alloys, the kinetics of such ordering is still not clear and more importantly its effect on the resulting mechanical properties, not to mention the salient mechanisms involved, is still a contentious issue. Without such information, it is still not known whether the notion of "tailoring disorder with order" is a viable proposition for improving the properties of these alloys.

Declaration of competing interest

The authors declare that they have no known competing financial interests or personal relationships that could have appeared to influence the work reported in this paper.

Acknowledgements

FCGF is grateful for the support of the Brazilian agencies FAPERJ (E-26/200.650/2021), CAPES (88881.361735/2019-01), and CNPq (140178/2019-8). MAM thanks the Center for Matter in Extreme Conditions (award number DE-NA0003842) for its support on the dynamic performance of HEAs. ROR acknowledges support from the Damage-Tolerance in Structural Materials program at the Lawrence Berkeley National Laboratory which is funded by the U.S. Department of Energy, Office of Science, Office of Basic Energy Sciences, Materials Sciences and Engineering Division, under contract no. DE-AC02-05-CH11231.

REFERENCES

[1] He Q, Ding Z, Ye Y, Yang Y. Design of high-entropy alloy: a perspective from nonideal mixing. J Occup Med 2017;69(11):2092–8.
[2] Cantor B, Chang I, Knight P, Vincent A. Microstructural development in equiatomic multicomponent alloys. Mater Sci Eng 2004;375–377:213–8.
[3] Yeh J, Chen S, Lin S, Gan J, Chin T, Shun T, et al. Nanostructured high-entropy alloys with multiple principal elements: novel alloy design concepts and outcomes. Adv Eng Mater 2004;6(5):299–303.
[4] Chen T, Shun T, Yeh J, Wong M. Nanostructured nitride films of multi-element high-entropy alloys by reactive DC sputtering. Surf Coating Technol 2004;188–189:193–200.
[5] Hsu C, Yeh J, Chen S, Shun T. Wear resistance and high-temperature compression strength of FCC CuCoNiCrAl0.5Fe alloy with boron addition. Metall Mater Trans A 2004;35A:1465–9.
[6] Huang P, Yeh J, Shun T, Chen S. Multi-principal-element alloys with improved oxidation and wear resistance for thermal spray coating. Adv Eng Mater 2004;6:74–8.
[7] Yeh J, Chen S, Gan J, Lin S, Chin T, Shun T, et al. Formation of simple crystal structures in Cu-Co-Ni-Cr-Al-Fe-Ti-V. Metall Mater Trans 2004;35A:2533–6.
[8] Otto F, Yang Y, Bei H, George E. Relative effects of enthalpy and entropy on the phase stability of equiatomic high-entropy alloys. Acta Mater 2013;61:2628–38.
[9] Yeh J. Alloy design strategies and future trends in high-entropy alloys. J Occup Med 2013;65:1759–71.
[10] Yeh J. Physical metallurgy of high-entropy alloys. J Occup Med 2015;67:2254–61.
[11] Miracle D, Senkov O. A critical review of high entropy alloys and related concepts. Acta Mater 2017;122:448–511.
[12] George E, Raabe D, Ritchie RO. High-entropy alloys. Nat Rev Mater 2019;4:515–34.
[13] Miracle D, Miller J, Senkov O, Woodward C, Uchic M, Tiley J. Exploration and development of high entropy alloys for structural applications. Entropy 2014;16:494–525.
[14] Ye Y, Wang Q, Lu J, Liu C, Yang Y. High-entropy alloy: Challenges and prospects. Mater Today 2016;19:349–62.
[15] Garcia Filho F, Monteiro S. Welding joints in high entropy alloys: a short-review on recent trends. Materials 2020;13:1411.
[16] Zhang W, Liaw P, Zhang Y. Science and technology in high-entropy alloys. Science China Materials 2018;61:2–22.
[17] Diao H, Feng R, Dahmen K, Liaw P. Fundamental deformation behavior in high-entropy alloys: an overview. Curr Opin Solid State Mater Sci 2017;21(5):252–66.
[18] Zhang Y, Zuo T, Tang Z, Gao M, Dahmen K, Liaw P, et al. Microstructures and properties of high entropy alloys. Prog Mater Sci 2014;61:1–93.
[19] Tsai M, Yeh J. High-entropy alloys: a critical review. Materials Research Letter 2014;2:107–23. 2014.
[20] Li Z, Zhao S, Ritchie RO, Meyers M. Mechanical properties of high-entropy alloys with emphasis on face-centered cubic alloys. Prog Mater Sci 2019;102:296–345.
[21] George E, Curtin W, Tasan C. High entropy alloys: A focused review of mechanical properties and deformation mechanisms. Acta Mater 2020;188:435–74.
[22] Wu W, Ni S, Liu Y, Song M. Effects of cold rolling and subsequent annealing on the microstructure of a HfNbTaTiZr high-entropy alloy. J Mater Res 2016;31(24):3815–23.
[23] Zhao Y, Qiao J, Ma S, Gao M, Yang H, Chen M, et al. A hexagonal close-packed high-entropy alloy: the effect of entropy. Mater Des 2016;96:10–5.
[24] Li Z. Interstitial equiatomic CoCrFeMnNi high-entropy alloys: carbon content, microstructure, and compositional homogeneity effects on deformation behavior. Acta Mater 2019;164:400–12.
[25] Seol J, Bae J, Li Z, Han J, Kim J, Raabe D, et al. Boron doped ultrastrong and ductile high-entropy alloys. Acta Mater 2018;151:366–76.
[26] Stepanov N, Yurchenko N, Tikhonovsky M, Salishchev G. Effect of carbon content and annealing on structure and hardness of the CoCrFeNiMn-based high entropy alloys. J Alloys Compd 2016;687:59–71.
[27] Ye Y, Ouyang B, Liu C, Duscher G, Nieh T. Effect of interstitial oxygen and nitrogen on incipient plasticity of NbTiZrHf high-entropy alloys. Acta Mater 2020;199:413–24.
[28] Wang Z, Baker I, Cai Z, Chen S, Poplawsky J, Guo W. The effect of interstitial carbon on the mechanical properties and dislocation substructure evolution in Fe40.4Ni11.3Mn34.8Al7.5Cr6 high entropy alloy. Acta Mater 2016;120:228–39.
[29] Lei Z, Liu X, Wu Y, Wang H, Jiang S, Wang S, et al. Enhanced strength and ductility in high-entropy alloy via ordered oxygen complexes. Nature 2018;563:546–50.
[30] Pickering E, Munoz-Moreno R, Stone H, Jones N. Precipitation in the equiatomic high-entropy alloy CrMnFeCoNi. Scripta Mater 2016;113:106–9.
[31] Tsai M, Chang K, Li J, Tsai R, Cheng A. A second criterion for sigma phase formation in high entropy alloys. Mater. Res. Lett. 2016;4(2):90–5.
[32] Ming K, Bi XWJ. Precipitation strengthening of ductile Cr15Fe20Co35Ni20Mo10 alloys. Scripta Mater 2017;137:88–93.
[33] Vakili S, Zarei-Hanzaki A, Anoushe A, Abedi H, Mohammad-Ebrahimi M, Jaskari M, et al. Reversible dislocation movement, martensitic transformation and nano-twinning during elastic cyclic loading of a metastable high entropy alloy. Acta Mater 2020;185:474–92.
[34] Li Z, Tasan C, Pradeep K, Raabe D. A TRIP- assisted dual-phase high-entropy alloy: Grain size and phase fraction effects on deformation behavior. Acta Mater 2017;131:323–35.
[35] Li Z, Pradeep K, Deng Y, Raabe D, Tasan C. Metastable high-entropy dual-phase alloys overcome the strength-ductility trade-off. Nature 2016;534:227–30.
[36] Deng Y, Tasan C, Pradeep K, Springer H, Kostka A, Raabe D. Design of a twinning-induced plasticity high entropy alloy. Acta Mater 2015;94:124–33.
[37] Zhang Z, Sheng H, Wang Z, Gludovatz B, Zhang Z, George E, et al. Dislocation mechanisms and 3D twin architectures generate exceptional strength-ductility-toughness combination in CrCoNi medium-entropy alloy. Nat Commun 2017;8:14390.
[38] Cheng C, Yang Y, Zhong Y, Chen Y, Hsu T, Yeh J. Physical metallurgy of concentrated solid solutions from low-entropy to high-entropy alloys. Curr Opin Solid State Mater Sci 2017;21(6):299–311.
[39] Ye Y, Liu C, Yang Y. A geometric model for intrinsic residual strain and phase stability in high entropy alloys. Acta Mater 2015;94:152–61.
[40] King D, Middleburgh S, McGregor A, Cortie M. Predicting the formation and stability of single phase high-entropy alloys. Acta Mater 2016;104:172–9.
[41] Troparevsky M, Morris J, Kent P, Lupini A, Stocks G. Criteria for predicting the formation of single-phase high-entropy alloys. Phys Rev X 2015;5(1):11041. 0.
[42] Wang Z, Huang Y, Yang Y, Wang J, Liu C. Atomic-size effect and solid solubility of multicomponent alloys. Scripta Mater 2015;94:28–31.

[43] Senkov O, Miracle D. A new thermodynamic parameter to predict formation of solid solution or intermetallic phases in high entropy alloys. J Alloys Compd 2016;658:603–7.
[44] Poletti M, Battezzati L. Electronic and thermodynamic criteria for the occurrence of high entropy alloys in metallic systems. Acta Mater 2014;75:297–306.
[45] Guo S, Hu Q, Ng C, Liu C. More than entropy in high-entropy alloys: Forming solid solutions or amorphous phase. Intermetallics 2013;41:96–103.
[46] Tsai M, Tsai K, Tsai C, Lee C, Juan C, Yeh J. Criterion for sigma phase formation in Cr- and V- containing high-entropy alloys. Materials Research Letters 2013;1(4):207–12.
[47] Chou T, Huang J, Yang C, Lin S, Nieh T. Consideration of kinetics on intermetallics formation in solid-solution high entropy alloys. Acta Mater 2020;195:1–10.
[48] Chattopadhyay C, Prasad A, Murty B. Phase prediction in high entropy alloys - a kinetic approach. Acta Mater 2018;153:214–25.
[49] Hume-Rothery W, Coles B. The transition metals and their alloys. Adv Phys 1954;3(10):149–242.
[50] Zhang Y, Zhou Y, Lin J, Chen G, Liaw P. Solid-solution phase formation rules for multi-component alloys. Adv Eng Mater 2008;10(6):534–8.
[51] Yang X, Zhang Y. Prediction of high-entropy stabilized solid-solution in multi-component alloys. Mater Chem Phys 2012;132:233–8.
[52] Zhang Y, Yang X, Liaw P. Alloy design and properties optimization of high-entropy alloys. J Occup Med 2012;64:830–8.
[53] Guo s, Ng C, Lu J, Liu C. Effect of valence electron concentration on stability of fcc or bcc phase in high entropy alloys. Jounal of Applied Physics 2011;109(10):213.
[54] Zhu Z, Ma K, Wang Q, Shek C. Compositional dependence of phase formation and mechanical properties in three CoCrFeNi-(Mn/Al/Cu) high entropy alloys. Intermetallics 2016;79:1–11.
[55] Lyu Z, Lee C, Wang S, Fan X, Yeh J, Liaw P. Effects of constituent elements and fabrication methods on mechanical behavior of high-entropy alloys: A review. Metall Mater Trans 2019;50A:1–28.
[56] Cui P, Ma Y, Zhang L, Zhang M, Fan J, Dong W, et al. Effect of Ti on microstructures and mechanical properties of high entropy alloys based on CoFeMnNi system. Mater Sci Eng 2018;737:198–204.
[57] Dong Y, Lu Y, Jiang L, Wang T, Li T. Effects of electro-negativity on the stability of topologically close-packed phase in high entropy alloys. Intermetallics 2014;52:105–9.
[58] Vaidya M, Guruvidyathri K, Murty B. Phase formation and thermal stability of CoCrFeNi and CoCrFeMnNi equiatomic high entropy alloys. J Alloys Compd 2019;774:856–64.
[59] Divinski S, Lukianova O, Wilde G, Dash A, Esakkiraja N, Paul A. High-entropy alloys: diffusion. In: Encyclopedia of materials: metals and alloys; 2020. p. 1–18.
[60] Vaidya M, Trubel S, Murty B, Wilde G, Divinski S. Ni tracer diffusion in CoCrFeNi and CoCrFeMnNi high entropy alloys. J Alloys Compd 2016;688:994–1001.
[61] Nadutov V, Mazanko V, Makarenko S. Tracer diffusion of cobalt in high entropy alloys AlxFeNiCoCuCr. Metallofiz Noveishie Tekhnol 2017;39:337–48.
[62] Li Q, Chen W, Zhong J, Zhang L, Chen Q, Liu Z-K. On sluggish diffusion in fcc Al–Co–Cr–Fe–Ni high-entropy alloys: An experimental and numerical study. Metals 2017;8(1):16.
[63] Kulkarni K, Chauhan G. Investigations of quaternary interdiffusion in a constituent system of high entropy alloys. AIP Adv 2015;5(9):97162. 0.
[64] Esakkiraja N, Pandey K, Dash A, Paul A. Pseudo-binary and pseudo-ternary diffusion couple methods for estimation of the diffusion coefficients in multicomponent systems and high entropy alloys. Phil Mag 2019;99(18):2236–64.
[65] Esakkiraja N, Paul A. A novel concept of pseudo ternary diffusion couple for the estimation of diffusion coefficients in multicomponent systems. Scripta Mater 2018;147:79–82.
[66] Morral J. Body-diagonal diffusion couples for high entropy alloys. J Phase Equilibria Diffus 2018;39(1):51–6.
[67] Paul A. A pseudobinary approach to study interdiffusion and the Kirkendall effect in multicomponent systems. Phil Mag 2013;93(18):2297–315.
[68] Kucza W, Dabrowa J, Cieslak G, Berent K, Kulik T, Danielewski M. Studies of "sluggish diffusion" effect in Co-Cr-Fe-Mn-Ni, Co-Cr-Fe-Ni and Co-Fe-Mn-Ni high entropy alloys; determination of tracer diffusivities by combinatorial approach. J Alloys Compd 2018;731:920–8.
[69] Vaidya M, Pradeep K, Murty B, Wilde G, Divinski S. Radioactive isotopes reveal a non-sluggish kinetics of grain boundary diffusion in high entropy alloys. Sci Rep 2017;7(1):1–11.
[70] Gaertner D, Kottke J, Wilde G, Divinski S, Chumlyakov Y. Tracer diffusion in single crystalline CoCrFeNi and CoCrFeMnNi high entropy alloys. J Mater Res 2018;33(19):3184–91.
[71] Wu Z, Bei H, Otto F, Pharr G, George E. Recovery, recrystallization, grain growth and phase stability of a family of FCC-structured multi-component equiatomic solid solution alloys. Intermetallics 2014;46:131–40.
[72] Wu Z, Bei H, Pharr G, George E. Temperature dependence of the mechanical properties of equiatomic solid solution alloys with face-centered cubic crystal structures. Acta Mater 2014;81:428–41.
[73] Ondicho I, Choi M, Choi W, Jeon J, Jafarian H, Lee B, et al. Experimental investigation and phase diagram of CoCrMnNi-Fe system bridging high-entropy alloys and high-entropy steels. J Alloys Compd 2019;785:320–7.
[74] Kiran Kumar N, Li C, Leonard K, Bei H, Zinkle S. Microstructural stability and mechanical behavior of FeNiMnCr high entropy alloy under ion irradiation. Acta Mater 2016;113:230–44.
[75] Gigax J, El-Atwani O, McCulloch Q, Aytuna B, Efe M, Fensin S, et al. Micro- and mesoscale mechanical properties of an ultra-fine grained CrFeMnNi high entropy alloy produced by large strain machining. Scripta Mater 2020;178:508–12.
[76] Bracq G, Laurent-Brocq M, Perriere L, Pires R, Joubert J, Guillot I. The fcc solid solution stability in the Co-Cr-Fe-Mn-Ni multi-component system. Acta Mater 2017;128:327–36.
[77] Laplanche G, Gadaud P, Barsch C, Demtroder K, Reinhart C, Schreuer J, et al. Elastic moduli and thermal expansion coefficients of medium-entropy subsystems of the CrMnFeCoNi high-entropy alloy. J Alloys Compd 2018;746:244–55.
[78] Lucas M, Wilks G, Mauger L, Munoz J, Senkov O, Michel E, et al. Absence of long-range chemical ordering in equimolar FeCoCrNi. Applied Phsics Letters 2012;100:251907.
[79] Wu Y, Zhang F, Yuan X, Huang H, Wen X, Wang Y, et al. Short-range ordering and its effects on mechanical properties of high-entropy alloys. Mater Sci Technol 2021;62:214–20. https://doi.org/10.1016/j.jmst.2020.06.018.
[80] Singh P, Smirnov A, Johnson D. Atomic short-range order and incipient long-range order in high-entropy alloys. Phys Rev B 2015;91:224204.
[81] Ding J, Yu Q, Asta M, Ritchie RO. Tunable stacking fault energies by tailoring local chemical order in CrCoNi medium-entropy alloys. Proc Natl Acad Sci Unit States Am 2018;115(36):8919–24.
[82] Ma Y, Wang Q, Li C, Santodonato L, Feygenson M, Dong C, et al. Chemical short-range orders and induced structural

transition in high-entropy alloys. Scripta Mater 2018;144:64–8.
[83] Zhang R, Zhao S, Ding J, Chong Y, Jia T, Ophus C, et al. Short-range order and its impact on the CrCoNi medium-entropy alloy. Nature 2020;581:283–99.
[84] Laplanche G, Berlund S, Reinhart C, Kostka A, Fox F, George E. Phase stability and kinetics of delta-phase precipitation in CrMnFeCoNi high-entropy alloys. Acta Mater 2018;161:338–51.
[85] Otto F, Dlouhy A, Somsen C, Bei H, Eggeler G, George E. The influences of temperature and microstructure on the tensile properties of a CoCrFeMnNi high-entropy alloy. Acta Meterialia 2013;61(15):5743–55.
[86] Otto F, Dlouhy A, Pradeep K, Kubenova M, Raabe D, Eggeler G, et al. Decomposition of the single-phase high entropy alloy CrMnFeCoNi after prolonged anneals at intermediate temperatures. Acta Mater 2016;112:40–52.
[87] Vaidya M, Karati A, Marshal A, Pradeep K, Murty B. Phase evolution and stability of nanocrystalline CoCrFeNi and CoCrFeMnNi high entropy alloys. J Alloys Compd 2019;770:1004–15.
[88] Praveen S, Basu J, Kashyap S, Kottada R. Exceptional resistance to grain growth in nanocrystalline CoCrFeNi high entropy alloy at high homologous temperatures. J Alloys Compd 2016;662:361–7.
[89] He J, Wang H, Huang H, Xu X, Chen M, Wu Y, et al. A precipitation-hardened high-entropy alloy with outstanding tensile properties. Acta Mater 2016;102:187–96.
[90] He F, Wang Z, Cheng P, Wang Q, Li J, Dang Y, et al. Designing eutectic high entropy alloys of CoCrFeNiNbx. J Alloys Compd 2016;656:284–9.
[91] Dahlborg U, Cornide J, Calvo-Dahlborg M, Hansen T, Fitch A, Leong Z, et al. Structure of some CoCrFeNi and CoCrFeNiPd multicomponent HEA alloys by diffraction techniques. J Alloys Compd 2016;681:330–41.
[92] He F, Wang Z, Wu Q, Li J, Wang J, Liu C. Phase separation of metastable CoCrFeNi high entropy alloy at intermediate temperatures. Scripta Mater 2017;126:15–9.
[93] Porter D, Easterling K, Sherif M. In: Phase transformations in metals and alloys. 3rd ed. CRC Press; 2009. p. 536.
[94] Lin Q, Liu J, An X, Wang H, Zhang Y, Liao X. Cryogenic-deformation-induced phase transformation in an FeCoCrNi high-entropy alloy. Materials Research Letters 2018;6(4):236–43.
[95] Yang X, Sun S, Ruan H, Shi S, Zhang T. Shear and shuffling accomplishing polymorphic fcc $\gamma \rightarrow$ hcp $\varepsilon \rightarrow$ bct α martensitic phase transformation. Acta Mater 2017;136:347–54.
[96] Zhang F, Wu Y, Lou H, Zeng Z, Prakapenka V, Greenberg E, et al. Polymorphism in a high-entropy alloy. Nat Commun 2017;8:15687.
[97] Meyers M, Chawla K. In: Mechanical behavior of materials. 2nd ed. Cambridge University Press; 2008. p. 882.
[98] Zaddach A, Niu C, Koch C, Irving D. Mechanical properties and stacking fault energies of NiFeCrCoMn high-entropy alloy. J Occup Med 2013;65:1780–9.
[99] Zhang Y, Zhuang Y, Hu A, Kai J, Liu C. The origin of negative stacking fault energies and nano-twin formation in face-centered cubic high entropy alloys. Scripta Mater 2017;130:96–9.
[100] Kivy M, Zaeem M. Generalized stacking fault energies, ductilities, and twinnabilities of CoCrFeNi-based face-centered cubic high entropy alloys. Scripta Mater 2017;139:83–6.
[101] Gao M, Yeh J, Liaw P, Zhang Y, editors. High-entropy alloys. Springer International Publishing; 2016.
[102] Zhao Y, Yang T, Tong Y, Wang J, Luan J, Jiao Z, et al. Heterogeneous precipitation behavior and stacking-fault-mediated deformation in a CoCrNi-based medium -entropy alloy. Acta Mater 2017;138:72–82.
[103] Liu S, Wu Y, Wang H, He J, Liu J, Chen C, et al. Stacking fault energy of face-centered-cubic high entropy alloys. Intermetallics 2018;93:269–73.
[104] Ma Y, Yuan F, Yang M, Jiang P, Ma E, Wu X. Dynamic shear deformation of a CrCoNi medium-entropy alloy with heterogeneous grain structures. Acta Mater 2018:407–18.
[105] Wu X, Zhu Y, Wei Y, Wei Q. Strong strain hardening in nanocrystalline nickel. Phys Rev Lett 2009;103:205504.
[106] Dupuy L, Fivel M. A study of dislocation junctions in FCC metals by an orientation dependent line tension model. Acta Mater 2002;50:4873–85.
[107] Zhu L, Qu S, Guo X, Lu J. Analysis of the twin spacing and grain size effects on mechanical properties in hierarchically nanotwinned face-centered cubic metals based on a mechanism based plasticity model. J Mech Phys Solid 2015;76:162–79.
[108] Zhu L, Kou H, Lu J. On the role of hierarchical twins for achieving maximum yield strength in nanotwinned metals. Appl Phys Lett 2012;101:81906. 0.
[109] Jin W, Cheng G, Xu W, Yan H, Tsai M, Wang Q, et al. Ultrastrong Mg alloy via nano-spaced stacking faults. Mater. Res. Lett. 2013;1:61–6.
[110] Mao J, Slone C, Smith T, Niu C, Bei H, Ghazisaeidi M, et al. The evolution of the deformation substructure in a Ni-Co-Cr equiatomic solid solution alloy. Acta Mater 2017;132:35–48.
[111] Mani A, Salinas-Rodriguez LH. Deformation induced FCC to HCP transformation in a Co-27-Cr-5Mo-0.05C alloy. Mater Sci Eng 2011;528:3037–43.
[112] Li Z, Zhao S, Alotaibi S, Liu Y, Wang B, Meyers M. Adiabatic shear localization in the CrMnFeCoNi high-entropy alloy. Acta Mater 2018;151:424–31.
[113] Green M, Choi C, Hattrick-Simpers J, Joshi A, Takeuchi I, Barron S, et al. Fulfilling the promise of the materials genome initiative with high-throughput experimental methodologies. Appl Phys Rev 2017;4:11105. 0.
[114] Jian A, Persson K, Ceder G. Research update: the materials genome iniciative: data sharing and the impact of collaborative ab initio databases. Apl Mater 2016;4:53102. 0.
[115] Drosback M. Materials genome iniciative: advances and initiatives. J Occup Med 2014;66:334–5.
[116] Senkov O, Miller J, Miracle D, Woodward C. Accelerated exploration of multi-principal element alloys with solid solution phases. Nat Commun 2015;6:6529.
[117] Zhang C, Zhang F, Diao H, Gao M, Tang Z, Poplawsky J, et al. Understanding phase stability of Al-Co-Cr-Fe-Ni high entropy alloys. Mater Des 2016;109:425–33.
[118] Liu X, Sha G, Wu Q, Liang Y, Huang J, Jin K, et al. Phase stability of an high-entropy Al-Cr-Fe-Ni-V alloy with exceptional mechanical properties: First-principles and APT investigations. Comput Mater Sci 2019;170:109161.
[119] Singh P, Smirnov A, Alam A, Johnson D. First-principles prediction of incipient order in arbitrary high-entropy alloys: exemplified in Ti0.25CrFeNiAlx. Acta Mater 2020;189:248–54.
[120] Chen W, Ding X, Feng Y, Liu X, Liu K, Lu Z, et al. Vacancy formation enthalpies of high-entropy FeCoCrNi alloy via first-principles calculations and possible implications to its superior radiation tolerance. J Mater Sci Technol 2018;34(2):355–64.
[121] Niu C, Zaddach J, Koch C, Irving D. First principles exploration of near-equiatomic NiFeCrCo high entropy alloys. J Alloys Compd 2016;672:510–20.
[122] Alhafez I, Ruestes C, Bringa E, Urbassek H. Nanoindentation into a high-entropy alloy - an atomistic study. J Alloys Compd 2019;803:618–24.

[123] Liu J. Molecular dynamic study of temperature dependence of mechanical properties and plastic inception of CoCrCuFeNi high-entropy alloy. Phys Lett 2020;384(22):126516.
[124] Qi Y, Chen X, Feng M. Molecular dynamics-based analysis of the effect of voids and HCP-phase inclusion on deformation of single-crystal CoCrFeMnNi high-entropy alloy. Mater Sci Eng 2020;791:139444.
[125] Antillon E, Woodward C, Rao S, Akdim B, Parthasarathy T. Chemical short range order strengthening in a model FCC high entropy alloy. Acta Mater 2020;190:29–42.
[126] Durga A, Hari Kumar K, Murty B. Phase formation in equiatomic high entropy alloys: CALPHAD approach and experimental studies. Trans Indian Inst Met 2012;65:375–80.
[127] Thermo-Calc Software. Thermodynamic databases [Online]. Available: http://www.thermocalc.com/products-services/databases/thermodynamic/. [Accessed 21 May 2020].
[128] Zhang C, Zhang F, Chen S, Cao W. Computational thermodynamics aided high-entropy alloy design. J Occup Med 2012;64(7):839–45.
[129] Zhang F, Zhang C, Chen S, Zhu J, Cao W, Kattner U. An understanding of high entropy alloys from phase diagram calculations. Calphad 2014;45:1–10.
[130] Morral J, Chen S. A regular solution model for a single-phase high entropy and enthalpy alloy. J Phase Equilibria Diffus 2017;38(4):382–90.
[131] Pickering E, Jones N. High-entropy alloys: a critical assessment of their founding principles and future prospects. Int Mater Rev 2016;61(3):183–202.
[132] Fernandez-Caballero A, Fedorov M, Wrobel J, Mummery P, Nguyen-Manh D. Configurational entropy in multicomponent alloys: matrix formulation from Ab initio based Hamiltonian and application to the FCC CrFeMnNi system. Entropy 2019;21:68. 2019.
[133] Laplanche G, Kostka A, Reinhart C, Hunfeld J, Eggeler G, George E. Reasons for the superior mechanical properties of medium-entropy CrCoNi compared to high entropy CrMnFeCoNi. Acta Mater 2017;128:292–303.
[134] Gludovatz B, Hohenwater A, Thurston K, Bei H, Wu Z, George E, et al. Exceptional damage-tolerance of a medium-entropy alloy CrCoNi at cryogenic temperatures. Nat Commun 2016;7:10602.
[135] Tsai C, Lee C, Lin P, Xie X, S C, Carroll R, et al. Portevin-Le Chatelier mechanism in face-centered-cubic metallic alloys from low to high entropy. Int J Plast 2019;122:212–24.
[136] Kumar N, Ying Q, Nie X, Mishra R, Tang Z, Liaw P, et al. High strain-rate compressive deformation behavior of the Al0.1CrFeCoNi. Mater Des 2015;86:598–602.
[137] Sharma A, Singh P, Johnson D, Liaw P, Balasubramanian G. Atomistic clustering-ordering and high-strain deformation of an Al0.1CrCoFeNi high-entropy alloy. Sci Rep 2016;6:31028.
[138] Kuznetsov A, Shaysultanov D, Stepanov N, Salishchev G, Senkov O. Superplasticity of AlCoCrCuFeNi high entropy alloy. Mater Sci Forum 2013;735:146–51.
[139] Carroll R, Lee C, Tsai C, Yeh J, Antonaglia J, Brinkman B, et al. Experiments and model for serration statistics in low-entropy, medium-entropy and high-entropy alloys. Sci Rep 2015;5:16997.
[140] Yan N, Li Z, Xu Y, Meyers M. Shear localization in metallic materials at high strain rates. Prog Mater Sci 2021;119:100755.
[141] Li Z, Zhao S, Diao H, Liaw P, Meyers M. High-velocity deformation of Al0.3CoCrFeNi high-entropy alloy: Remarkable resistance to shear failure. Sci Rep 2017;7:42742.
[142] Fu A, Liu B, Li Z, Wang B, Cao Y, Liu Y. Dynamic deformation behavior of a FeCrNi medium entropy alloy. J Mater Sci Technol 2022;100:120–8.
[143] Ma Y, Yang M, Yuan F, Wu X. Deformation induced hcp nano-lamella and its size effect on the strengthening in a CoCrNi medium-entropy alloy. J Mater Sci Technol 2021;82:122–34.
[144] Lu P, Zhang T, Zhao D, Ma S, Li Q, Wang T, et al. Effects of stress states and strain rates on mechanical behavior and texture evolution of the CoCrFeNi high-entropy alloy: Experiment and simulation. J Alloys Compd 2021;851:156779.
[145] Shabani M, Indeck J, Hazeli K, Jablonski P, Pataky G. Effect of strain rate on the tensile behavior of CoCrFeNi and CoCrFeMnNi high-entropy alloys. J Mater Eng Perform 2019;28:4348–56.
[146] Komarasamy M, Kumar N, Mishra R, Liaw P. Anomalies in the deformation mechanism and kinetics of coarse-grained high entropy alloy. Mater Sci Eng, A 2016;654:256–63.
[147] Moon J, Hong S, Bae J, Jang M, Yim D, Kim H. On the strain rate-dependent deformation mechanism of CoCrFeMnNi high-entropy alloy at liquid nitrogen temperature. Mater. Res. Lett. 2017;5:427–77.
[148] Gao T, D Z, Zhang T, Jin T, Ma S, Wang Z. Strain-rate-sensitive mechanical response, twinning, and texture features of NiCoCrFe high-entropy alloy: Experiments, multi-level crystal plasticity and artificial neural networks modeling. J Alloys Compd 2020;845:155911.
[149] Zhao S, Li Z, Zhu C, Yang W, Zhang Z, Armstrong D, et al. Amorphization in extreme deformation of the CrMnFeCoNi high-entropy alloy. Sci Adv 2021;7(5).
[150] Laplanche G, Kostka A, Horst O, Eggeler G, George E. Microstructure evolution and critical stress for twinning in the CrMnFeCoNi high-entropy alloy. Acta Mater 2016;118:152–63.
[151] Jang M, Ahn D-H, Moon J, Bae J, Yim D, Yeh J-W, et al. Constitutive modeling of deformation behavior of high-entropy alloys with face-centered cubic crystal structure. Mater. Res. Lett. 2017;5:350–6.
[152] Jian W, Xie Z, Xu S, Yao X, Beyerlein I. Shock-induced amorphization in medium entropy alloy CoCrNi. Scripta Mater 2022;209:114379.
[153] Tsai M. Three strategies for the design of advanced high-entropy alloys. Entropy 2016;18(252):e1870252.
[154] Tian F, Varga L, Chen N, Shen J, Vitos L. Empirical design of single phase high-entropy alloys with high hardness. Intermetallics 2015;58:1–6.
[155] Erdogan A, Yener T, Zeytin S. Fast production of high entropy alloys (CoCrFeNiAlxTiy) by electric current activated sintering system. Vacuum 2018;155:64–72.
[156] Yang T, Zhao Y, Tong Y, Jiao Z, Wei J, Cai J, et al. Multicomponent intermetallic nanoparticles and superb mechanical behaviors of complex alloys. Science 2018;362:933–7.
[157] Jin X, Liang Y, Zhang L, Bi J, Zhou Y, Li B. Back stress strengthening dual phase AlCoCr2FeNi2 high entropy alloy with outstanding tensile properties. Mater Sci Eng 2019;745:137–43.
[158] Liu D, Zhao J, Li Y, Zhu W, Lin L. Effects of boron content on microstructure and wear properties of FeCoCrNiBx high-entropy alloy coating by laser cladding. Appl Sci 2020;10:49.
[159] Li Z, Tasan C, Springer H, Gault B, Raabe D. Interstitial atoms enable joint twinning and transformation induced plasticity in strong and ductile high-entropy alloys. Sci Rep 2017;7:40704.

[160] Song M, Zhou R, Gu J, Wang Z, Ni S, Liu Y. Nitrogen induced heterogeneous structures overcome strength-ductility trade-off in an additively manufactured high-entropy alloy. Applied Materials Today 2020;18:100498.
[161] Yang F, Dong L, Hu X, Zhou X, Fang F, Xie Z, et al. Microstructural features and tensile behaviors of a novel FeMnCoCr high entropy alloys. Mater Lett 2020;275:128154.
[162] Wang Z, Baker I, Cai Z, Chen S, Poplawsky J, Guo W. The effectof interstitial carbon on the mechanical properties and dislocation substructure evolution in Fe40.4Ni11.3Mn34.8Al7.5Cr6 high entropy alloys. Acta Mater 2016;120:228–39.
[163] Lei Z, Liu X, Wu Y, Wang H, Jiang S, Wang S, et al. Enhanced strength and ductility in a high-entropy alloy via ordered oxygen complexes. Nature 2018;563:546–50.
[164] Liu X, Liu L, Liu G, Wu X, Lu D, Yao J, et al. The role of carbon in grain refinement of cast CrFeCoNi high-entropy alloys. Metall Mater Trans 2018;49:2151–60.
[165] Li Z. Interstitial equiatomic CoCrFeMnNi high-entropy alloys: carbon content, microstructure, and compositional homogenity effects on deformation behavior. Acta Mater 2019;164:400–12.
[166] Liu W, Lu Z, He J, Luan J, Wang Z, Liu B, et al. Ductile CoCrFeNiMox high entropy alloys strengthened by hard intermetallic phases. Acta Mater 2016;116:332–42.
[167] Wang W, Wang W, Wang S, Tsai Y, Lai C, Yeh J. Effects of Al addition on the microstructure and mechanical property of AlxCoCrFeNi high-entropy alloys. Intermetallics 2012;26:44–51.
[168] Du C, Hu L, PAn Q, Chen K, Zhou P, Wang G. Effect of Cu on the strengthening and embrittling of an FeCoNiCr-xCu HEA. Mater Sci Eng, A 2022;832:142413.
[169] Tong Y, Chen D, Han B, Wang J, Feng R, Yang T, et al. Outstanding tensile properties of a precipitation-strengthened FeCoNiCrTi0.2 high-entropy alloy at room and cryogenic temperatures. Acta Mater 2019;165:228–40.
[170] Chung D, Kwon H, Eze C, Kim W, Na Y. Influence of Ti addition on the strengthening and toughening effect in CoCrFeNiTix multi principal element alloys. Metals 2021;11(10):1511.
[171] Qi Y, He T, Feng M. The effect of Cu and Mn elements on the mechanical properties of single-crystal CoCrFeNi-based high-entropy alloy under nanoindentation. J Appl Phys 2021;129:195104.
[172] Salishchev G, Tikhonovsky M, Shaysultanov D, Stepanov N, Kuznetsov A, Kolodiy I, et al. Effect of Mn and V on structure and mechanical properties of high-entropy alloys based on CoCrFeNi system. J Alloys Compd 2014;591:11–21.
[173] Yin B, Maresca F, Curtin W. Vanadium is an optimal element for strengthening in both fcc and bcc high-entropy alloys. Acta Mater 2020;188:486–91.
[174] Stepanov N, Shaysultanov D, Salishchev G, Tikhonovsky M, Oleynik E, Tortika A, et al. Effect of V content on microstructure and mechanical properties of the CoCrFeMnNiVx high entropy alloys. J Alloys Compd 2015;628:170–85.
[175] Sunkari U, Reddy S, Athira K, Chatterjee S, Bhattacharjee P. Effect of niobium alloying on the microstructure, phase stability and mechanical properties of CoCrFeNi2.1Nbx high entropy alloys: Experimentation and thermodynamic modeling. Mater Sci Eng, A 2020;793:139897.
[176] Sunkari U, Reddy S, Chatterjee S, Bhattacharjee P. Effect of prolonged aging on phase evolution and mechanical properties of intermetallic strengthened CoCrFeNi2.1Nbx high entropy alloys. Mater Lett 2019;248:119–22.
[177] Zhou K, Li J, Wang L, Yang H, Wang Z, Wang J. Direct laser deposited bulk CoCrFeNiNbx high entropy alloys. Intermetallics 2019;114:106592.
[178] Fleischer R. Substitutional solution hardening. Acta Metall 1963;11:203–9.
[179] Varvenne C, Luque A, Curtin W. Theory of strengthening in fcc high entropy alloys. Acta Mater 2016;118:164–76.
[180] Li J, Jia W, Wang J, Kou H, Zhang D, Beugnon E. Enhanced mechanical properties of a CoCrFeNi high entropy alloy by supercooling method. Mater Des 2016;95:183–7.
[181] Linder T, Lobel M, Sattler B, Lampke T. Surface hardening of FCC phase high-entropy alloy system by powder-pack boriding. Surf Coating Technol 2019;371:389–94.
[182] Cheng Z, Zhu W, Yang L, Zhao C, Wei P, Ren F. Tuning the mechanical properties of Fex(CoMoNi)100-x high-entropy alloys via controlled formation of hard μ phase. Mater Sci Eng 2020;773:138881.
[183] Liang D, Zhao C, Zhu W, Wei P, Jiang F, Zhang Y, et al. Overcoming the strength-ductility trade-off via the formation of nanoscale Cr-rich precipitates in an ultrafine-grained FCC CrFeNi medium entropy alloy matrix. Mater Sci Eng 2019;762:138107.
[184] Zheng F, Zhang G, Chen X, Yang X, Yang Z, Li Y, et al. A new strategy of tailoring strength and ductility of CoCrFeNi based high-entropy alloy. Mater Sci Eng 2020;774:138940.
[185] Han B, Wei J, Tong Y, Chen D, Zhao Y, Wang J, et al. Composition evolution of gamma prime nanoparticles in the Ti-doped CoFeCrNi high entropy alloy. Scripta Mater 2018;148:42–6.
[186] Niu S, Kou H, Guo T, Zhang Y, Wang J, Li J. Strengthening of nano-precipitations in an annealed Al0.5CoCrFeNi high entropy alloy. Mater Sci Eng 2016;671:82–6.
[187] Yang W, Qu P, Sun J, Yue Q, Su H, Zhang J, et al. Effect of alloying elements on stacking fault energies of γ and γ' phases in Ni-based superalloy calculated by first principles. Vacuum 2020;181:109682.
[188] Takasugi T, Izumi O, Masahashi N. Electronic and structural studies of grain boundary strength and fracture in L12 ordered alloys - II. On the effect of third elements in Ni3Al alloy. Acta Metall 1985;33(7):1259–69.
[189] Chun J, Byrne J, Bornemann A. The inhibition of deformation twinning by precipitates in a magnesium-zinc alloy. Phil Mag: A Journal of Theoretical Experimental and Applied Physics 1969;20(164):291–300.
[190] Jain J, Poole W, Sinclair C, Gharghouri M. Reducing the tension-compression yield asymmetry in a Mg-8Al-0.5Zn alloy via precipitation. Scripta Mater 2010;62:301–4.
[191] Kovarik L, Unocic R, Li J, Sarosi P, Shen C, Wang Y, et al. Micro-twinning and other shearing mechanisms at intermediate temperatures in Ni-based superalloys. Prog Mater Sci 2009;54(6):839–73.
[192] Yang T, Zhao Y, Liu W, Kai J, Liu C. L12-strengthened high-entropy alloys for advanced structural applications. J Mater Res 2018;33(19):2983–97.
[193] He J, Wang H, Wu Y, Liu X, Mao H, Nieh T, et al. Precipitation behavior and its effects on tensile properties of FeCoNiCr high-entropy alloys. Intermetallics 2016;79:41–52.
[194] Shun T, Chang L, Shiu M. Microstructure and mechanical properties of multiprincipal component CoCrFeNiMox alloys. Mater Char 2012;70:63–7.
[195] Liu W, He J, Huang H, Wang H, Lu Z, Liu C. Effects of Nb additions on the microstructure and mechanical property of CoCrFeNi high-entropy alloys. Intermetallics 2015;60:1–8.
[196] He F, Wang Z, Niu S, Wu Q, Li J, Wang J, et al. Strengthening the CoCrFeNiNb0.25 high entropy alloy by FCC precipitate. J Alloys Compd 2016;667:53–7.
[197] Jiang H, Jiang L, Qiao D, Lu Y, Wang T, Cao Z, et al. Effect of niobium on microstructure and properties of the CoCrFenbxNi high entropy alloys. J Mater Sci Technol 2017;33:712–7.

[198] Wang Z, Zhou W, Fu L, Wang J, Luo R, Han X, et al. Effect on coherent L12 nanoprecipitates on the tensile behavior of a fcc-based high-entropy alloy. Mater Sci Eng 2017;696:503–10.
[199] Rehman H, Durst K, Neumeier S, Parsa A, Kostka A, Eggeler G, et al. Nanoindentation studies of the mechanical properties of the μ phase in a creep deformed Re containing nickel-based superalloy. Mater Sci Eng 2015;634:202–8.
[200] Huo W, Liu X, Tan S, Fang F, Xie Z, Shang J, et al. Ultrahigh hardness and high electrical resistivity in nano-twined nanocrystalline high-entropy alloy filmas. Appl Surf Sci 2018;439:222–5.
[201] Huo W, Fang F, Zhou H, Xie Z, Shang J, Jiang J. Remarkable strength of CoCrFeNi high-entropy alloy wires at cryogenic and elevated temperatures. Scripta Mater 2017;141:125–8.
[202] Fu Z, Chen W, Wen H, Zhang D, Chen Z, Zheng Y, et al. Microstructure and strengthening mechanisms in an FCC structured single-phase nanocrystalline Co25Ni25Fe25Al7.5Cu17.5 high-entropy alloy. Acta Mater 2016;107:59–71.
[203] Tang Q, Huang Y, Huang Y, Liao X, Langdon T, Dai P. Hardening of an Al0.3CoCrFeNi high entropy alloy via high-pressure torsion and thermal annealing. Mater Lett 2015;151:126–9.
[204] Schuh B, Mendez-Martin F, Volker B, George E, Clemens H, Pippan R, et al. Mechanical properties, microstructure and thermal stability of a nanocrystalline CoCrFeMnNi high-entropy alloy after severe plastic deformation. Acta Mater 2015;96:258–68.
[205] Reddy T, Wani I, Bhattacharjee T, Reddy S, Saha R, Bhattacharjee P. Severe plastic deformation driven nanostructure and phase evolution in a Al0.5CoCrFeMnNi dual phase high entropy alloy. Intermetallics 2017;91:150–7.
[206] Cizek J, Hausld P, Cieslar M, Melikhova O, Vlasak T, Janecek M, et al. Strength enhancement of high entropy alloy HfNbTaTiZr by severe plastic deformation. J Alloys Compd 2018;768:924–37.
[207] Gubicza J, Hung P, Kawasaki M, Han J, Zhao Y, Xue Y, et al. Influence of severe plastic deformation on the microstructure and hardness of a CoCrFeNi high-entropy alloy: A comparison with CoCrFeNiMn. Mater Char 2019;154:304–14.
[208] Yoshida S, Bhattacharjee T, Bai Y, Tsuji N. Friction stress and Hall-Petch relationship in CoCrNi equiatomic medium entropy alloy processed by severe plastic deformation and subsequent annealing. Scripta Mater 2017;134:33–6.
[209] Shahmir H, He J, Lu Z, Kawasaki M, Langdon T. Effect of annealing on mechanical properties of a nanocrystalline CoCrFeNiMn high-entropy alloy processed by high-pressure torsion. Mater Sci Eng 2016;676:294–303.
[210] Lu W, Luo X, Yang Y, Huang B. Hall-petch relationship and heterogeneous strength of CocrNi medium-entropy alloy. Mater Chem Phys 2020;251:123073.
[211] Yang M, Yan D, Yuan F, Jiang P, Ma E, Wu X. Dynamically reinforced heterogeneous grain structure prolongs ductility in a medium-entropy alloy with gigapascal yield strength. Proc Natl Acad Sci Unit States Am 2018;115(28):7224–9.
[212] Yang M, Pan Y, Yuan F, Zhu Y, Wu X. Back stress strengthening and strain hardening in gradient structure. Materials Research Letters 2016;4(3):145–51.
[213] Huang C, Wang Y, Ma X, Yin S, Hoppel H, Goken M, et al. Interface affected zone for optimal strength and ductility in heterogeneous laminate. Mater Today 2018;21(7):713–9.
[214] Wu X, Zhu Y. Heterogeneous materials: a new class of materials with unprecedented mechanical properties. Materials Research Letters 2017;5(8):527–32.
[215] Yang M, Yuan F, Xie Q, Wang Y, Ma E, Wu X. Strain hardening in Fe-16Mn-10Al-0.86C-5Ni high specific strength steel. Acta Mater 2016;109:213–22.
[216] Han Q, Asgari A, Hodgson P, Stanford N. Strain partitioning in dual-phase steels containing tempered martensite. Mater Sci Eng, A 2014;611:90–9.
[217] Cong Z, Jia N, Sun X, Ren Y, Almer J, Wang Y. Stress and strain partitioning of ferrite and martensite during deformation. Metall Mater Trans 2009;40:1383–7.